

Orbital currents and charge density waves in a generalized Hubbard ladder

J. O. Fjærestad,^{1,2} J. B. Marston,³ and U. Schollwöck⁴

¹*Department of Physics and Astronomy, University of California, Los Angeles, California 90095, USA*

²*Department of Physics, University of Queensland, Brisbane, Qld 4072, Australia*

³*Department of Physics, Brown University, Providence, Rhode Island 02912, USA*

⁴*Institute for Theoretical Physics C, RWTH Aachen, D-52056 Aachen, Germany*

(Dated: March 23, 2022)

We study a generalized Hubbard model on the two-leg ladder at zero temperature, focusing on a parameter region with staggered flux (SF)/d-density wave (DDW) order. To guide our numerical calculations, we first investigate the location of a SF/DDW phase in the phase diagram of the half-filled weakly interacting ladder using a perturbative renormalization group (RG) and bosonization approach. For hole doping δ away from half-filling, finite-size density-matrix renormalization-group (DMRG) calculations are used to study ladders with up to 200 rungs for intermediate-strength interactions. In the doped SF/DDW phase, the staggered rung current and the rung electron density both show periodic spatial oscillations, with characteristic wavelengths $2/\delta$ and $1/\delta$, respectively, corresponding to ordering wavevectors $2k_F$ and $4k_F$ for the currents and densities, where $2k_F = \pi(1 - \delta)$. The density minima are located at the anti-phase domain walls of the staggered current. For sufficiently large dopings, SF/DDW order is suppressed. The rung density modulation also exists in neighboring phases where currents decay exponentially. We show that most of the DMRG results can be qualitatively understood from weak-coupling RG/bosonization arguments. However, while these arguments seem to suggest a crossover from non-decaying correlations to power-law decay at a length scale of order $1/\delta$, the DMRG results are consistent with a true long-range order scenario for the currents and densities.

PACS numbers: 71.10.Fd, 71.10.Hf, 71.10.Pm, 71.30.+h

I. INTRODUCTION

The possibility of finding new phases of matter is a major motivation behind the study of materials of strongly correlated electrons. A phase with staggered orbital currents which was first considered theoretically in 1968¹ and then rediscovered two decades later^{2,3,4,5,6} has lately been the subject of a revival of interest, mainly due to recent proposals^{7,8} that the pseudogap region⁹ in the phase diagram of the cuprate high-temperature superconductors may be characterized by this kind of order, either long-ranged (i.e., a true broken-symmetry state),⁷ or fluctuating.⁸ This orbital current phase is known variously as the orbital antiferromagnet, staggered flux (SF) or d-density wave¹⁰ (DDW) phase; in this paper we will refer to it as the SF/DDW phase. The long-range ordered version of this phase breaks the rotational and translational symmetries of the underlying Hamiltonian, in addition to time reversal symmetry. The fundamental experimental signature of the long-range-ordered SF/DDW scenario with ordering wavevector (π, π) is an elastic Bragg peak at that wavevector in neutron scattering.^{6,11} The results of some recent neutron scattering experiments on underdoped $\text{YBa}_2\text{Cu}_3\text{O}_{6+x}$ have been argued to be consistent with this scenario.^{11,12,13} A different circulating-current broken-symmetry state with a current pattern that does not break translational symmetry has also been proposed for the pseudogap phase in the cuprates.¹⁴

It is important to acquire an understanding of what kinds of microscopic models can give rise to a SF/DDW ground state. For models of interacting fermions in two spatial dimensions this issue has been addressed by many

authors^{2,3,4,5,6,15,16,17,18,19,20,21,22,23,24,25} using a variety of methods. While the two-dimensional case is the most relevant one for the cuprates, the behavior of strongly correlated electrons in two dimensions is still a subject that is marred by great controversy. In a few special model cases the fermion sign problem is absent and thus quantum Monte Carlo simulations can be done reliably, leading among other things to interesting findings with regard to SF/DDW order²⁵ and also more exotic current-carrying states.²⁶ However, in the vast majority of cases, and certainly for the models and parameter values that are expected to be most relevant for real materials, the available analytical and numerical methods are only approximate, and their reliability is difficult to gauge.

In contrast, the fact that many powerful methods exist for one spatial dimension has enabled much solid knowledge to be established about strongly correlated one-dimensional systems, and it is hoped that some of this may also be relevant for the behavior of correlated electrons in two dimensions. In this regard, two-leg Hubbard and t - J ladders have attracted much interest, as it has been found that these models have a spin gap and that upon doping away from half-filling the dominant correlations are d -wave-like superconducting correlations,²⁷ two features which are reminiscent of the pseudogap and the $d_{x^2-y^2}$ symmetry of the superconducting state in the cuprates, respectively. Ladder systems are also interesting in their own right, not least due to experimental realizations of such materials. The most well-known example, $\text{Sr}_{14-x}\text{Ca}_x\text{Cu}_{24}\text{O}_{41}$, contains two-leg ladder substructures, and has been found to have a spin gap, and to become superconducting upon doping

at high pressure.^{27,28}

The possibility of having SF/DDW order in two-leg ladders has also received much attention recently.^{29,30,31,32,33,34,35,36,37,38,39,40,41} The two-leg ladder is the simplest geometry that can support a SF/DDW phase, with currents flowing around the elementary square plaquettes. In this paper we present an extensive study of SF/DDW order in generalized Hubbard ladders, focusing mainly on the case of finite hole doping away from half-filling. Some of the results that will be discussed have been briefly presented in Ref. 39.

We first use bosonization and a perturbative renormalization-group (RG) approach to identify a parameter region with long-range SF/DDW order in the weakly interacting half-filled ladder.^{35,37,38} Finite-system density-matrix renormalization-group (DMRG) calculations are then used to study the SF/DDW phase in doped ladders, for intermediate-strength interactions and ladder sizes up to 200 rungs. For the (rational) hole dopings considered, currents are found to be large (of order the nearest-neighbor hopping amplitude t) and show no evidence of decay. As the doping is increased the currents in the SF/DDW phase decrease in magnitude, and for sufficiently strong doping SF/DDW order becomes completely suppressed. The SF/DDW phase has a spin gap, but d -wave-like superconducting correlations decay exponentially.

In the half-filled SF/DDW phase, the sign of the rung current changes from one rung to the next, while the magnitude stays the same, corresponding to an ordering wavevector $2k_F = \pi$ in the direction parallel to the legs. In contrast, the rung currents found in the doped SF/DDW phase vary both in sign and magnitude, corresponding to an ordering wavevector $2k_F = \pi(1 - \delta) \neq \pi$, where δ is the hole doping away from half-filling. Such phases are often referred to as incommensurate. An incommensurate SF/DDW phase has been suggested as a candidate for the hidden order in the heavy fermion compound URu₂Si₂.⁴² Incommensurate SF/DDW phases have also been studied in various two-dimensional models.^{16,23,43} [A note on terminology: In the remainder of this paper only ordering patterns with an infinite unit cell will be characterized as ‘incommensurate;’ orderings with a finite unit cell (even when it is very large) will be referred to as ‘commensurate.’ The former (latter) case includes orderings with wavevector $2k_F = \pi(1 - \delta)$ with δ an irrational (rational) number.]

Charge density wave order in ladder systems is also a topic that has attracted much interest recently, both theoretically^{37,38,44,45,46,47,48} and experimentally.^{49,50,51,52,53,54} Interestingly, we find that a charge density modulation coexists with the orbital currents in the doped SF/DDW phase. Like the currents, this density modulation is not found to decay. The staggered rung current and the rung electron density both show a periodic spatial variation, with characteristic wavelengths $2/\delta$ and $1/\delta$, respectively. The den-

sity modulation corresponds to an ordering wavevector $4k_F$, with two doped holes (one per leg) per wavelength. Furthermore, the minima of the electron density are located at the zeros of the staggered rung current. In other words, the rungs at which the doped holes predominantly sit are antiphase domain walls for the current pattern. This property, and the related factor of two ratio between the periods of the staggered rung current and the rung electron density, are very reminiscent of the properties of stripe phases with coexisting spin and charge order in doped antiferromagnets,⁵⁵ in which the role of the current in the SF/DDW phase is played by the spin density. The rung density modulation is found to persist in the neighboring phases of the SF/DDW phase in the phase diagram in which current correlations decay exponentially. We note that coexistence of current and charge order for an SF/DDW phase in two dimensions with ordering wavevector $\mathbf{q} \neq (\pi, \pi)$ for the currents has previously been discussed within the framework of a phenomenological mean-field approach.⁴³

Is the current and charge density order long-ranged? The DMRG calculations do seem to support a commensurate true long-range order scenario. Let us first note that, to the best of our knowledge, such a scenario does not violate any exact theorems that are directly applicable to the lattice model studied here; in particular, the Mermin-Wagner theorem is respected. Of course, these nonviolation arguments do not say whether or not true long-range order actually will occur. A weak-coupling RG/bosonization analysis of the continuum limit of the lattice model predicts that (1) true long-range order requires Umklapp interactions to be relevant in the RG sense, (2) at half-filling, Umklapp interactions are relevant, resulting in true long-range order,^{35,37,38} (3) for dopings away from half-filling Umklapp interactions are irrelevant, and as a result correlation functions decay as power laws (for distances much larger than $1/\delta$ ³⁷), i.e., only quasi long-range order is predicted.^{35,37} DMRG calculations find true long-range order at half-filling,³⁶ thus agreeing with the RG/bosonization analysis in that case. But as already noted, DMRG calculations seem to support a true long-range order scenario also for the doped ladder. We have not been able to resolve this apparent discrepancy between the predictions of the DMRG and RG/bosonization methods, and can only speculate about its origin. Both methods have their limitations and weaknesses. One particular question mark associated with the weak-coupling RG/bosonization method is whether its predictions regarding the range of the order may be unreliable for the ladders studied here with DMRG, for which the interactions are not weak. But one certainly cannot exclude the possibility that there may be a different and perhaps quite subtle reason for the discrepancy. We refer the reader to the concluding Sec. VI for an attempt at a fuller discussion of these issues.

The paper is organized as follows. The generalized Hubbard model on the two-leg ladder is introduced in Sec. II. In Sec. III we use a perturbative RG ap-

proach and bosonization to study the phase diagram of the model for weak interactions at half-filling. In Sec. IV we present an extensive DMRG study of the model for nonzero doping and intermediate-strength interactions. In Sec. V the doped ladder is discussed using weak-coupling RG and bosonization arguments. Sec. VI contains a summary and concluding discussion. Some details of the RG/bosonization calculations are discussed in three appendices. Throughout the paper the main focus is on the SF/DDW phase, but properties of neighboring phases in the phase diagram are also discussed.

II. MODEL

The model we will study is an “extended” or “generalized” Hubbard model with various nearest-neighbor interactions in addition to the on-site Hubbard term. For the purpose of finding SF/DDW order, it is necessary to allow for these additional interactions because the ground states of the pure Hubbard ladder and the related t - J ladder have been found to only have short-ranged SF/DDW correlations.^{33,36} Another, more general, motivation for studying generalized Hubbard models is that, although much attention has been paid over the years to the two-dimensional Hubbard and t - J models as purportedly “minimal” effective models for describing the physics of the two-dimensional CuO_2 planes in the cuprate superconductors, there is an increasing amount of studies that suggest that these models do not support high-temperature superconductivity.^{56,57}

The Hamiltonian of our model is $H = H_0 + H_I$, where the kinetic energy and interaction operators are, respectively,

$$\begin{aligned} H_0 &= -t \sum_{xs} \left(\sum_{\ell} c_{\ell, x+1, s}^{\dagger} c_{\ell x s} + c_{t x s}^{\dagger} c_{b x s} \right) + \text{H.c.}, \\ H_I &= \sum_x \left(\sum_{\ell} [U n_{\ell, x, \uparrow} n_{\ell, x, \downarrow} + V_{\parallel} n_{\ell x} n_{\ell, x+1} \right. \\ &\quad \left. + J_{\parallel} \mathbf{S}_{\ell x} \cdot \mathbf{S}_{\ell, x+1}] + V_{\perp} n_{t x} n_{b x} + J_{\perp} \mathbf{S}_{t x} \cdot \mathbf{S}_{b x} \right). \end{aligned} \quad (2.1)$$

The operator $c_{\ell x s}^{\dagger}$ creates an electron on rung $x = 1, \dots, L$ on the “top” or “bottom” leg $\ell = t, b$ with spin $s = \uparrow, \downarrow$, and obeys $\{c_{\ell x s}, c_{\ell' x' s'}^{\dagger}\} = \delta_{\ell \ell'} \delta_{x x'} \delta_{s s'}$. Electrons can hop between nearest-neighbor sites along legs and rungs with hopping amplitude t . Electron density operators are given by $n_{\ell x s} = c_{\ell x s}^{\dagger} c_{\ell x s}$ and $n_{\ell x} = \sum_s n_{\ell x s}$, and the spin operator is $\mathbf{S}_{\ell x} = \frac{1}{2} \sum_{ss'} c_{\ell x s}^{\dagger} \boldsymbol{\sigma}_{ss'} c_{\ell x s'}$, where the σ^i are Pauli matrices. The interactions consist of the Hubbard on-site term with strength U , as well as nearest-neighbor density-density and spin exchange interactions with strength V_{\perp} and J_{\perp} along the rungs, and V_{\parallel} and J_{\parallel} along the legs. As the leg interactions will be seen to favor other phases than SF/DDW, we will in most of the paper take $V_{\parallel} = J_{\parallel} = 0$.

III. WEAKLY INTERACTING ELECTRONS ON THE HALF-FILLED LADDER

In this section we study the case of weakly interacting electrons on a half-filled ladder.^{35,37,38,58} The fermionic perturbative RG approach of Refs. 58,59,60 is employed to obtain a low-energy effective theory which is then analyzed using bosonization and semiclassical considerations. Our focus is on finding a parameter regime for which the model (2.1) has a ground state with long-ranged SF/DDW order. The phase diagrams obtained for the weakly interacting half-filled ladder serve as helpful guides in the search for SF/DDW order in the doped ladder for intermediate interaction strengths, using the DMRG method, as described in Sec. IV. Furthermore, some of the results established here are used in the RG/bosonization analysis of the doped ladder in Sec. V.

A. Continuum description

To study the weak-interaction problem, we first diagonalize the kinetic energy. As it is convenient to deal with a translationally invariant Hamiltonian, we impose periodic boundary conditions in the direction parallel to the legs. By introducing even and odd combinations $c_{\lambda x s} = (c_{t x s} + (-1)^{\lambda} c_{b x s})/\sqrt{2}$ with $\lambda = 1, 2$, and Fourier transforming along the leg direction, the kinetic energy is diagonalized in momentum space, describing an anti-bonding band ($\lambda = 1$) and a bonding band ($\lambda = 2$), with dispersions $\varepsilon_{\lambda}(k) = -2t \cos k - (-1)^{\lambda} t$ (we set the lattice constant equal to 1). The Fermi level of the noninteracting half-filled system is at zero energy and crosses both bands, thus giving rise to four Fermi points $\pm k_{F1,2}$ which satisfy

$$k_{F1} + k_{F2} = \pi. \quad (3.1)$$

As interactions are assumed to be weak, we focus on states very close to the Fermi energy, and linearize the kinetic energy around the Fermi points. The band operator $c_{\lambda x s}$ can be expressed as a sum of right-moving (R) and left-moving (L) components,

$$c_{\lambda x s} = \sum_P e^{i P k_F \lambda x} \psi_{P \lambda s}(x), \quad (3.2)$$

where $P = R, L \equiv \pm 1$. The continuum fields $\psi_{P \lambda s}(x)$ are slowly varying on the scale of the lattice constant. The linearized kinetic energy can be written $H_0 = \int dx \mathcal{H}_0$, where

$$\mathcal{H}_0 = -i v_F \sum_{P \lambda s} P \psi_{P \lambda s}^{\dagger} \partial_x \psi_{P \lambda s}, \quad (3.3)$$

where the Fermi velocity is $v_F = \sqrt{3}t$.

Interactions will scatter electrons between the Fermi points. Introducing the “currents”⁵⁹

$$J_{\lambda P} = \sum_s \psi_{P \lambda s}^{\dagger} \psi_{P \lambda s}, \quad \mathbf{J}_{\lambda P} = \frac{1}{2} \sum_{ss'} \psi_{P \lambda s}^{\dagger} \boldsymbol{\sigma}_{ss'} \psi_{P \lambda s'},$$

$$L_P = \sum_s \psi_{P1s}^\dagger \psi_{P2s}, \quad \mathbf{L}_P = \frac{1}{2} \sum_{ss'} \psi_{P1s}^\dagger \boldsymbol{\sigma}_{ss'} \psi_{P2s'},$$

$$M_{\lambda P} = -i\psi_{P\lambda\uparrow} \psi_{P\lambda\downarrow}, \quad N_{Pss'} = \psi_{P1s} \psi_{P2s'}, \quad (3.4)$$

the Hamiltonian density that describes the effects of the weak interactions to leading order can be written $\mathcal{H}_I = \mathcal{H}_I^{(1)} + \mathcal{H}_I^{(2)}$, where

$$\mathcal{H}_I^{(1)} = -g_{1\rho} \sum_\lambda J_{\lambda R} J_{\lambda L} - g_{x\rho} (J_{1R} J_{2L} + J_{2R} J_{1L})$$

$$- g_{1\sigma} \sum_\lambda \mathbf{J}_{\lambda R} \cdot \mathbf{J}_{\lambda L} - g_{x\sigma} (\mathbf{J}_{1R} \cdot \mathbf{J}_{2L} + \mathbf{J}_{2R} \cdot \mathbf{J}_{1L})$$

$$- g_{t\rho} (L_R L_L + L_R^\dagger L_L^\dagger) - g_{t\sigma} (\mathbf{L}_R \cdot \mathbf{L}_L + \mathbf{L}_R^\dagger \cdot \mathbf{L}_L^\dagger), \quad (3.5)$$

$$\mathcal{H}_I^{(2)} = -g_{xu} (M_{1R} M_{2L}^\dagger + M_{2R} M_{1L}^\dagger)$$

$$- \sum_{ss'} (g_{tu1} N_{Rss'} N_{Lss'}^\dagger + g_{tu2} N_{Rss'} N_{Ls's}^\dagger) + \text{H.c.} \quad (3.6)$$

Here $\mathcal{H}_I^{(2)}$ represents (interband) Umklapp interactions.

B. Bosonization

Bosonization proves very helpful for interpreting the low-energy effective theory resulting from the perturbative RG flow (see Sec. III C). In the Abelian bosonization formalism^{61,62,63,64,65} the fermionic field operators $\psi_{P\lambda s}$ can be expressed in terms of dual or conjugate Hermitian bosonic fields $\phi_{\lambda s}$ and $\theta_{\lambda s}$ as

$$\psi_{P\lambda s} = \frac{1}{\sqrt{2\pi\alpha}} \eta_{\lambda s} \exp[i(P\phi_{\lambda s} + \theta_{\lambda s})], \quad (3.7)$$

where α is a short-distance cutoff. The only equal-time nonzero commutator between the bosonic fields is (taking the limit $\alpha/(x-x') \rightarrow 0$)

$$[\phi_{\lambda s}(x), \theta_{\lambda' s'}(x')] = i\pi \delta_{\lambda\lambda'} \delta_{ss'} H(x-x'), \quad (3.8)$$

where $H(x)$ is the Heaviside step function. The long-wavelength normal-ordered fermionic densities can be expressed in terms of the bosonic fields as

$$\psi_{P\lambda s}^\dagger \psi_{P\lambda s} = \frac{1}{2\pi} \partial_x (\phi_{\lambda s} + P\theta_{\lambda s}). \quad (3.9)$$

For later use we also define

$$\mathcal{N}_{P\lambda s} \equiv \int_0^L dx \psi_{P\lambda s}^\dagger \psi_{P\lambda s}. \quad (3.10)$$

The (Majorana) Klein factors^{61,64} $\eta_{\lambda s}$ in Eq. (3.7) commute with the bosonic fields, and satisfy $\{\eta_{\lambda s}, \eta_{\lambda' s'}\} = 2\delta_{\lambda\lambda'} \delta_{ss'}$. The Klein factor conventions used for the Hamiltonian and the order parameters considered in this paper (see below) are explained in Appendix A.

Charge (ρ) and spin (σ) operators are defined as $\phi_{\lambda\rho} = (\phi_{\lambda\uparrow} + \phi_{\lambda\downarrow})/\sqrt{2}$, $\phi_{\lambda\sigma} = (\phi_{\lambda\uparrow} - \phi_{\lambda\downarrow})/\sqrt{2}$. It is convenient to make a further change of basis, to $\phi_{r\nu} = (r\phi_{1\nu} +$

$\phi_{2\nu})/\sqrt{2}$, where $r = \pm$ and $\nu = \rho, \sigma$. Similar definitions apply to the θ -operators. In the (r, ν) -basis, the kinetic energy density reads

$$\mathcal{H}_0 = \frac{v_F}{2\pi} \sum_{r\nu} [(\partial_x \phi_{r\nu})^2 + (\partial_x \theta_{r\nu})^2]. \quad (3.11)$$

Furthermore, $\mathcal{H}_I^{(1)} = \mathcal{H}_I^{(1a)} + \mathcal{H}_I^{(1b)}$, where

$$\mathcal{H}_I^{(1a)} = \frac{1}{2\pi^2} \sum_{r\nu} g_{r\nu} [(\partial_x \phi_{r\nu})^2 - (\partial_x \theta_{r\nu})^2], \quad (3.12)$$

$$\mathcal{H}_I^{(1b)} = \frac{1}{(2\pi\alpha)^2} \left\{ 2 \cos 2\phi_{+\sigma} \left[g_{1\sigma} \cos 2\phi_{-\sigma} \right. \right.$$

$$+ g_{x\sigma} \cos 2\theta_{-\sigma} - g_{t\sigma} \cos 2\theta_{-\rho} \left. \right] - \cos 2\theta_{-\rho}$$

$$\left. \left[(g_{t\sigma} - 4g_{t\rho}) \cos 2\phi_{-\sigma} + (g_{t\sigma} + 4g_{t\rho}) \cos 2\theta_{-\sigma} \right] \right\}, \quad (3.13)$$

with $g_{r\rho} \equiv -(g_{1\rho} + r g_{x\rho})$ and $g_{r\sigma} \equiv -\frac{1}{4}(g_{1\sigma} + r g_{x\sigma})$. Finally, the Umklapp interaction density reads

$$\mathcal{H}_I^{(2)} = \frac{4}{(2\pi\alpha)^2} \cos 2\phi_{+\rho} \left[g_{xu} \cos 2\theta_{-\rho} + g_{tu1} \cos 2\phi_{-\sigma} \right.$$

$$+ (g_{tu1} + g_{tu2}) \cos 2\phi_{+\sigma} + g_{tu2} \cos 2\theta_{-\sigma} \left. \right]. \quad (3.14)$$

C. Perturbative renormalization group approach

The “bare” values of the nine coupling constants g_i in the continuum field theory can be expressed in terms of the interaction parameters in Eq. (2.1), and equations describing the RG flow (to one loop) of these coupling constants near the noninteracting fixed point can be derived⁵⁹ (see Appendix B). These RG equations are then solved numerically for given sets of initial conditions. Typically, it is found that as the length scale is increased, some of the couplings grow (sometimes after a sign change), while other couplings remain small.

The couplings which grow to be large (i.e., of order 1, at which point the numerical integration must be stopped since the perturbative RG equations are only valid for weak coupling) will tend to lock some of the bosonic fields in the minima of the cosine potentials in the Hamiltonian. In fact, in the parameter region considered in this paper, at half-filling one of the conjugate fields $\phi_{r\nu}$ and $\theta_{r\nu}$ in each sector $r\nu$ always becomes locked. These locked (and thus also gapped) operator fields can then be approximated by their c-number expectation values (integer multiples of $\pi/2$ for the Hamiltonian considered above), while their conjugate fields will fluctuate wildly. To deduce the nature of the ground state, it is necessary to bosonize various order parameters and use the information about the field-locking pattern to deduce which, if any, of these order parameters are nonzero, or have the most slowly decaying correlations.

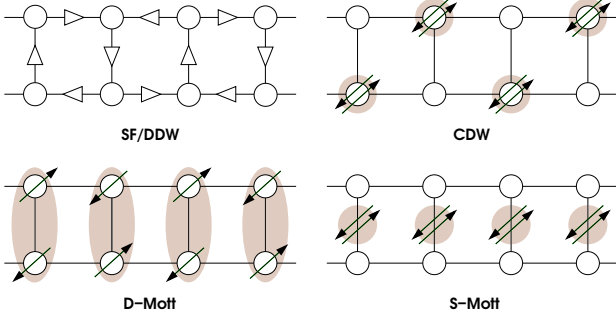


FIG. 1: Schematic illustration of phases at half-filling in the strong-coupling limit. Open (filled) arrows represent currents (spins). The shading indicates singlet pairs.

D. Phases, physical observables, and order parameters

As our main interest here is the SF/DDW phase, we will focus on a parameter region where this kind of order is realized. Three other phases will also be seen to be present in this parameter region in the weakly interacting half-filled ladder. These are the CDW, D-Mott, and S-Mott phases.⁶⁶ The nature of these four phases, most easily understood in the strong-coupling limit,^{38,58,67,68} is illustrated schematically in Fig. 1. These phases are all completely gapped, i.e., both charge sectors $\pm\rho$ and both spin sectors $\pm\sigma$ are gapped. Recently it has been shown that the two-leg ladder also can support four other completely gapped phases at half-filling,^{37,38} but none of these additional phases appear in the parameter region studied here.

We now discuss in some detail the various phases and the order parameters/physical observables that characterize them, *at half-filling*^{35,37,38,58} (the bosonized form of these physical observables in the *doped* ladder will be discussed in Sec. V A). In the SF/DDW phase, currents flow around the plaquettes as shown in Fig. 1. The ordering wavevector of the currents is $(q_x, q_y) = (\pi, \pi)$, where q_x (q_y) is the wavevector in the direction parallel (perpendicular) to the legs. The order parameter of this phase is

$$O_{\text{SF/DDW}} = \cos \phi_{+\rho} \cos \phi_{+\sigma} \cos \theta_{-\rho} \cos \theta_{-\sigma} + \sin \phi_{+\rho} \sin \phi_{+\sigma} \sin \theta_{-\rho} \sin \theta_{-\sigma}. \quad (3.15)$$

Denoting the rung current by $j_{\perp}(x)$, and defining the *staggered* rung current as

$$j_s(x) \equiv (-1)^x j_{\perp}(x), \quad (3.16)$$

we have $\langle j_s(x) \rangle \propto \langle O_{\text{SF/DDW}}(x) \rangle$; note that the expectation values are independent of x .

In the CDW phase the electron density exhibits a checkerboard pattern. This charge density order is thus characterized by the same ordering wavevector (π, π) as the currents in the SF/DDW phase. The order parameter is

$$O_{\text{CDW}} = \cos \phi_{+\rho} \cos \phi_{+\sigma} \sin \theta_{-\rho} \cos \theta_{-\sigma}$$

$$- \sin \phi_{+\rho} \sin \phi_{+\sigma} \cos \theta_{-\rho} \sin \theta_{-\sigma}. \quad (3.17)$$

In the CDW phase the expectation value of the deviation $\delta n_{\ell}(x)$ of the charge density at leg ℓ , rung x from the average density is given by $\langle \delta n_{\ell,b}(x) \rangle \propto \pm(-1)^x \langle O_{\text{CDW}}(x) \rangle$.

Both the SF/DDW and CDW phase spontaneously break a Z_2 symmetry, and thus have a two-fold degenerate ground state with true long-range order. This is intimately related to the fact that the order parameters of these phases depend on $\phi_{+\rho}$ which is locked by the Umklapp interaction, Eq. (3.14). In contrast, the D-Mott and S-Mott phases do not break any symmetry, but are characterized by a unique ground state with exponentially decaying *d*-wave-like and *s*-wave-like superconducting (SC) correlations, respectively. The pairing operators can be taken to be

$$\Delta_{\text{DSC/SSC}}(x) = (\psi_{R1\uparrow}\psi_{L1\downarrow} + \psi_{L1\uparrow}\psi_{R1\downarrow}) \mp (\psi_{R2\uparrow}\psi_{L2\downarrow} + \psi_{L2\uparrow}\psi_{R2\downarrow}). \quad (3.18)$$

In Δ_{DSC} the components of bands 1 and 2 (corresponding to transverse wavevector π and 0, respectively) come with opposite signs, while in Δ_{SSC} they have the same sign; this justifies calling these operators *d*- and *s*-wave-like, respectively. One finds that $\langle \Delta_a(x) \Delta_a^\dagger(0) \rangle \propto \langle O_a(x) O_a^\dagger(0) \rangle$, where $a = \text{DSC or SSC}$, and the order parameters are

$$O_{\text{DSC}} = e^{i\theta_{+\rho}} (\cos \phi_{+\sigma} \cos \theta_{-\rho} \cos \phi_{-\sigma} - i \sin \phi_{+\sigma} \sin \theta_{-\rho} \sin \phi_{-\sigma}), \quad (3.19)$$

$$O_{\text{SSC}} = e^{i\theta_{+\rho}} (\sin \phi_{+\sigma} \cos \theta_{-\rho} \sin \phi_{-\sigma} - i \cos \phi_{+\sigma} \sin \theta_{-\rho} \cos \phi_{-\sigma}). \quad (3.20)$$

The exponential decay of the pairing correlations comes from the $e^{i\theta_{+\rho}}$ factor, as $\theta_{+\rho}$ is conjugate to the locked field $\phi_{+\rho}$.

The field-locking patterns that realize the SF/DDW and CDW phases are easily deduced from their respective order parameters. Due to the absence of $\phi_{+\rho}$ in the DSC and SSC order parameters, the value of $\langle \phi_{+\rho} \rangle$ in the D-Mott and S-Mott phases must either be determined from the RG flow, or it can be deduced from the fact that the SF/DDW and the CDW phase can be regarded as the Ising-ordered counterparts of the quantum disordered D-Mott and S-Mott phase, respectively.³⁸ Field-locking patterns for the four phases are given in Table I.

E. Weak-coupling phase diagrams

Fig. 2(a) shows the phase diagram for $J_{\parallel} = V_{\parallel} = 0$ and $V_{\perp} > 0$ in the weak-coupling limit.³⁹ For the region $U > 0$ we may compare our results to those in Ref. 38 and find excellent agreement. The SF/DDW phase appears between the D-Mott and CDW phases and is seen to extend well beyond the region where it was first realized to exist,^{35,36} which was characterized by exact or approximate $\text{SO}(5)$ symmetry^{58,68} (the $\text{SO}(5)$ symmetry

Phase	$\langle\phi_{+\rho}\rangle$	$\langle\phi_{+\sigma}\rangle$	$\langle\theta_{-\rho}\rangle$	$\langle\theta_{-\sigma}\rangle$	$\langle\phi_{-\sigma}\rangle$
SF/DDW	0, π	0	0	0	\sim
CDW	0, π	0	$\pi/2$	0	\sim
D-Mott	0	0	0	\sim	0
S-Mott	0	0	$\pi/2$	\sim	0

TABLE I: Field-locking patterns (only unique up to a global gauge transformation of the fields) characterizing the ground states of the four phases encountered at half-filling. The two-fold degeneracy of the SF/DDW and CDW ground states has been reflected in the two values given for $\langle\phi_{+\rho}\rangle$. As $\theta_{-\sigma}$ and $\phi_{-\sigma}$ are conjugate fields, it follows that if one of them is locked, the other is strongly fluctuating; this is indicated by ‘ \sim ’.

occurs along the dotted line in the figure). The nature of the quantum phase transitions between the various phases has been discussed in detail in Refs. 37,38 (see also Ref. 58).

Next, we consider the effects of including interactions along the legs. We fix $U/V_{\perp} = 0.25$ and add a finite J_{\parallel}/V_{\perp} (Fig. 2(b)) or V_{\parallel}/V_{\perp} (Fig. 2(c)). J_{\parallel}/V_{\perp} is seen to favor the D-Mott phase. This squeezes the SF/DDW phase which eventually disappears for large enough values of J_{\parallel}/V_{\perp} . On the other hand, V_{\parallel}/V_{\perp} is seen to favor the CDW phase, which is easy to understand intuitively. However, in this case the SF/DDW order is more robust: the width of the SF/DDW region remains more or less constant as V_{\parallel}/V_{\perp} is increased, while its location is pushed towards larger values of J_{\perp}/V_{\perp} .

From Fig. 2 the conditions that favor SF/DDW order for repulsive interactions and positive exchange constants can be roughly summarized as follows:³⁸ the ratios J_{\perp}/U and V_{\perp}/U must be sufficiently large, but not too large (as that favors the D-Mott and CDW phase respectively), with leg interactions J_{\parallel} and V_{\parallel} preferably zero or at least small compared to the other interaction parameters. One might speculate that the reason why anisotropic interactions are required to stabilize SF/DDW order in the two-leg ladder could be related to the fact that the currents in the SF/DDW phase must themselves be anisotropic in this geometry in order to satisfy current conservation (the rung currents are twice as large as the leg currents). It is also interesting to note that in mean-field^{4,24} and renormalization-group^{21,22} studies of generalized Hubbard models on the square lattice in two dimensions, at or near half-filling, and with *isotropic* interactions (i.e., $J_{\perp} = J_{\parallel} = J$ and $V_{\perp} = V_{\parallel} = V$), the conditions that are most favorable for SF/DDW ordering tendencies also appear to be that the ratios J/U and $4V/U$ be sufficiently large.

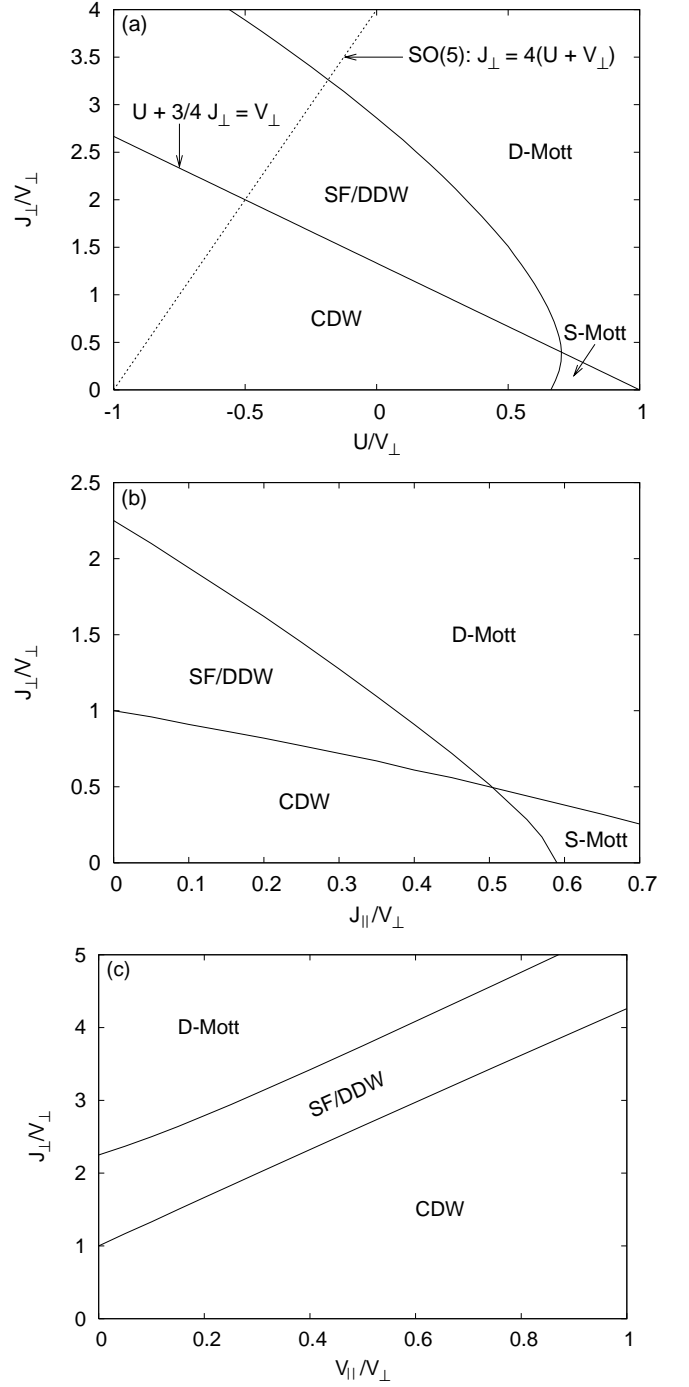


FIG. 2: Weak-coupling phase diagrams at half-filling, for $V_{\perp} > 0$. Of the four phases (illustrated in Fig. 1) that appear in these phase diagrams, the SF/DDW and CDW phase have true long-range order. The SF/DDW phase appears between the CDW and D-Mott phase. (a) $J_{\parallel} = V_{\parallel} = 0$. The half-filled model has SO(5) symmetry along the dashed line. The phase boundary line $U + (3/4)J_{\perp} = V_{\perp}$ is independent of the filling and valid for arbitrary interaction strengths, as shown in Refs. 40,41. (b) $V_{\parallel} = 0$, $U/V_{\perp} = 0.25$. (c) $J_{\parallel} = 0$, $U/V_{\perp} = 0.25$.

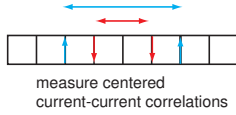


FIG. 3: (Color online) In real-valued DMRG, possible long-ranged current patterns are detected by calculating current-current correlations centered around the ladder middle.

IV. DMRG STUDY OF THE DOPED LADDER

In this section we discuss an extensive DMRG^{69,70,71} study of the ground state of hole-doped two-leg ladders with up to 200 rungs for intermediate interaction strengths. The doping away from half-filling is measured by the parameter δ , defined as

$$\delta \equiv 1 - n = \frac{\mathcal{N}_h}{2L}, \quad (4.1)$$

where n is the average number of electrons per site, and \mathcal{N}_h and L are the number of (doped) holes and rungs, respectively. Open boundary conditions were used, as these are computationally preferable in DMRG. The weak-coupling phase diagrams at half-filling discussed in Sec. III E were used as guides to suggest interesting parameter regimes.

To detect the existence of orbital currents, we have considered two approaches:

(i) Within a standard DMRG calculation in real number space, we have studied the decay of rung-rung correlations where the rungs have been centered about the middle of the ladder to minimize boundary effects (Fig. 3):

$$C(r) = \langle j_{\perp}(L/2 + r/2) j_{\perp}(L/2 - r/2) \rangle, \quad (4.2)$$

where the rung current $j_{\perp}(x) = \mathcal{J}_{(t,x),(b,x)}$ and the current operator between two nearest-neighbor sites \mathbf{i} and \mathbf{j} is given by

$$\mathcal{J}_{\mathbf{i},\mathbf{j}} = it \sum_s \left(c_{\mathbf{i},s}^{\dagger} c_{\mathbf{j},s} - c_{\mathbf{j},s}^{\dagger} c_{\mathbf{i},s} \right). \quad (4.3)$$

(ii) Within a DMRG calculation generalized to complex number space, one may obtain non-vanishing current expectation values,

$$\langle \mathcal{J}_{\mathbf{i},\mathbf{j}} \rangle \neq 0. \quad (4.4)$$

In the textbook case of a ferromagnet that develops a finite magnetization while spontaneously breaking the continuous rotational symmetry, this is achieved in theoretical approaches by forcing a possible symmetry breaking by introducing an infinitesimally strong external field.⁷² In close analogy, we break the Z_2 symmetry of the direction of plaquette currents by introducing an infinitesimal surface current $-h j_{\perp}(1)$ on the first rung of the ladder, corresponding to a weak surface field (Fig. 4). To assure

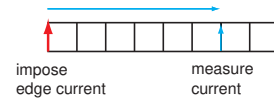


FIG. 4: (Color online) In complex-valued DMRG, possible long-ranged current patterns are detected by introducing a symmetry-breaking infinitesimal surface current and observing whether it sustains a long-ranged current pattern.

that this infinitesimal surface (or edge) current does not change the physics of the ladder under study, we have taken it down to values of $0.0001t$ (in some special cases even lower values were checked). We find that results do not change qualitatively while decreasing the surface current: in the phase that does support SF/DDW order, the magnitude of the orbital current measured numerically does not depend on its value in the small current limit, while in the phases that do not support SF/DDW order, the current decays exponentially fast into the bulk and its magnitude is proportional to the applied surface current.

For a large number of cases, we have performed both calculations and found results in very good agreement. However, the first approach, while computationally much less expensive, shows, due to the open boundary conditions used in the DMRG runs, much more pronounced finite-size effects: SF/DDW correlations are suppressed, not enhanced by the presence of open boundary conditions. Long-ranged or quasi-long-ranged order is thus often much harder to detect. Figs. 5 and 6 show the current-current correlations for a point in parameter space which exhibits SF/DDW order both for 8 and 12 percent doping and various ladder lengths. In the first case, correlations are weakly suppressed by the edges and order is demonstrated in agreement with the second approach; in the latter, correlations are strongly suppressed by the edges and grow strongly in size with ladder length; even for 200 rungs, it would be impossible to detect long-ranged order which is clearly visible from 50 rungs upwards in the second approach. For parameter sets where accessible system sizes allow to see long-ranged correlations also in the rung-rung current correlations, the values of the rung currents that can be extracted are in very good agreement with the values found by imposing an infinitesimal edge current.

In the second, computationally much harder, approach, we also observe that on very short ladders right at the CDW-SF/DDW phase boundary the open boundary conditions strongly favor a checkerboard charge density wave over the SF/DDW currents (Fig. 7), but the magnitude of the plaquette currents stabilizes very quickly with increasing system length, such that we have preferred this approach in our numerical calculations. In Refs. 40,41 exact duality relations were used to ascertain that the phase boundary between the SF/DDW and CDW phases lies at $U - V_{\perp} + (3/4)J_{\perp} = 0$. It is remarkable that, as evident in Fig. 7, strong currents are

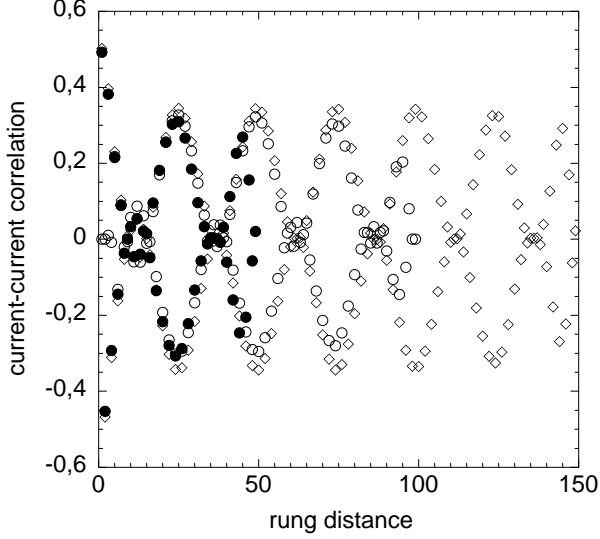


FIG. 5: Rung current-current correlations $C(r)$ calculated for ladders of length 50 (solid circles), 100 (open circles), 150 (diamonds) in the SF/DDW phase for $U = -0.4$, $t = 1$, $V_{\perp} = 0.9$, $J_{\perp} = 2$, and doping $\delta = 0.08$. $J_{\parallel} = V_{\parallel} = 0$ in this and all other figures in this section.

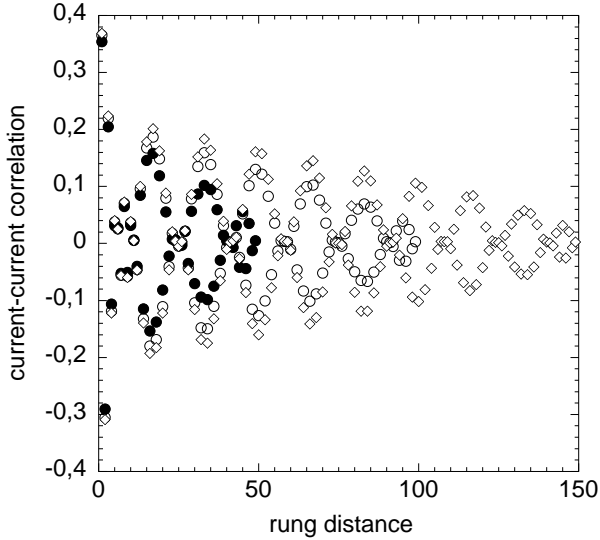


FIG. 6: Rung current-current correlations $C(r)$ as in Figure 5, but doping $\delta = 0.12$.

found to persist right at the phase boundary separating the SF/DDW and CDW phases. In this particular calculation, we have taken the edge current as small as $10^{-8}t$ without observing any change in the results.

The SF/DDW phase can be clearly distinguished from the neighboring CDW and doped D-Mott phases.⁷³ In both the CDW (Fig. 8) and doped D-Mott (Fig. 9) phase, the edge current induces rung currents $j_{\perp}(x)$ that die out exponentially fast, while in the SF/DDW phase it stabilizes a rung current orders of magnitude larger (Fig. 10). In the SF/DDW phase the *staggered* rung current

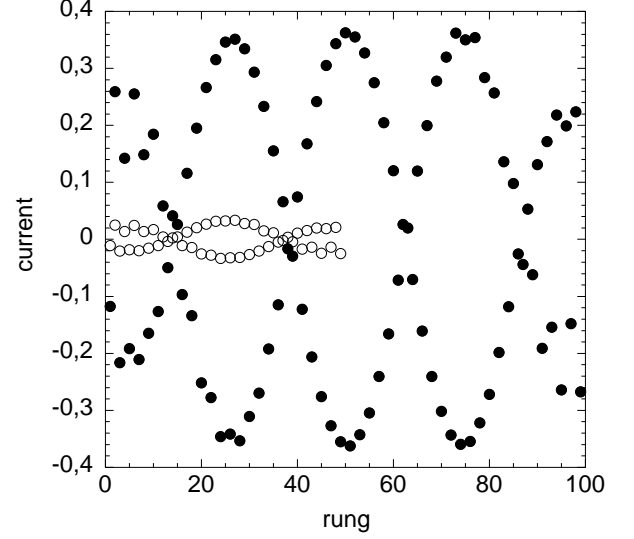


FIG. 7: Rung current at the phase boundary between SF/DDW and CDW order. The edge current is $0.0001t$ and $U = 0.25$, $t = V_{\perp} = 1$, $J_{\perp} = 1$, and doping $\delta = 0.04$ for ladder lengths 50 (open circles) and 100 (solid circles).

$j_s(x)$ (defined in Eq. (3.16)) oscillates around zero with a characteristic wavelength $2/\delta$ (this wavelength tends to decrease slightly with decreasing distance to the boundary). Thus the rung currents have anti-phase domain walls separated by a characteristic distance $1/\delta$. At these domain walls (or “discommensurations”) the rung current has the same sign on adjacent rungs ($++$ or $--$) instead of alternating between rungs as in the (“commensurate”) regions between domain walls. Furthermore, using that

$$2k_F \equiv k_{F1} + k_{F2} = \pi n = \pi(1 - \delta), \quad (4.5)$$

which is the generalization of Eq. (3.1) away from half-filling, one observes that the rung current oscillations may be associated with the fundamental wavevector $2k_F$ as these oscillations vary approximately as $\cos 2k_F x = (-1)^x \cos \pi \delta x$ (this equality holds since the rung index x is an integer). Moreover, the currents on the top and bottom leg are always opposite in sign. Consequently, the ordering wavevector of the currents is $(2k_F, \pi)$, which reduces to (π, π) at half-filling, as expected.

A modulation of the rung charge density coexists with the orbital currents in the SF/DDW phase (Fig. 10). The characteristic wavelength of this modulation is $1/\delta$ (again, the wavelength decreases slightly as the distance to the boundary decreases), which is just the average distance $L/(\mathcal{N}_h/2)$ between *pairs* of doped holes. Thus there are two doped holes per wavelength, one per leg; in a cartoon picture the doped hole pairs simply distribute themselves equidistantly along the ladder, each hole pair occupying one rung. These hole pairs tend to stay in the vicinity of the rung current minima (the domain walls of the current pattern). The ordering wavevector for this charge density modulation is $(4k_F, 0)$ because its charac-

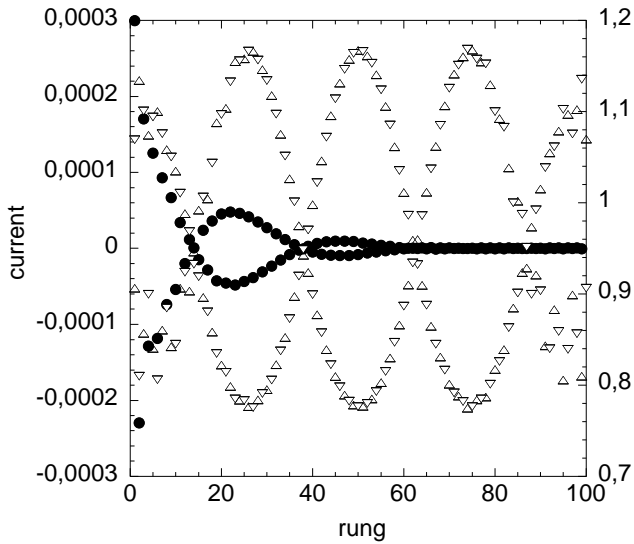


FIG. 8: Rung current (solid circles, left y -axis, units of t) and electronic densities on top and bottom ladder leg (up and down triangles, right y -axis) for 100 rung-ladder in the CDW phase and edge current $0.0001t$ ($U = 0.25$, $t = V_{\perp} = 1$, $J_{\perp} = 0.8$, and doping $\delta = 0.04$).

teristic periodicity in the direction parallel to the legs is the same as that of $\cos 4k_F x = \cos 2\pi\delta x$, and the density is the same on the top and bottom site of a rung. Clearly, this charge density modulation disappears at half-filling.

As seen in Fig. 9, the $(4k_F, 0)$ modulation of the charge density exists also in the doped D-Mott phase. The nature of the charge density pattern in the CDW phase (Fig. 8) is less obvious at first sight; however, as will become apparent in Sec. V, it is the sum of a large component with wavevector $(2k_F, \pi)$ and a smaller component with wavevector $(4k_F, 0)$. Thus the $(4k_F, 0)$ charge density modulation is present in all three phases appearing in the parameter region considered here. Such $(4k_F, 0)$ charge density modulations in two-leg ladders have recently been discussed by White *et al.*; ⁴⁵ we will analyze these modulations in more detail in Sec. V.

We have also calculated the DSC correlations in the SF/DDW and doped D-Mott phases (Fig. 11). In the SF/DDW phase the DSC correlations decay exponentially. As expected, the DSC correlations fall off more slowly in the doped D-Mott phase. Close to the phase boundary to the SF/DDW phase the correlations appear still to be exponential, however, while further into the doped D-Mott phase the edge effects make it difficult to say whether for longer system sizes the correlations might turn out to be algebraic.

Most of our DMRG calculations are for particle densities close to half-filling. As DMRG is a canonical ensemble method, particle numbers are fixed at each growth step and there is some arbitrariness in inserting the particles and holes to maintain essentially constant particle density during system growth. Various insertion schemes have yielded essentially identical results. To obtain such

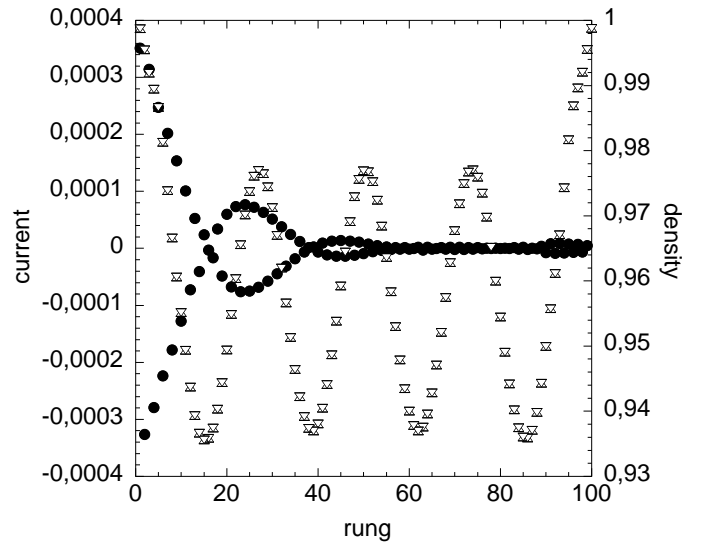


FIG. 9: Rung current (solid circles, left y -axis, units of t) and electronic densities on top and bottom ladder leg (up and down triangles, right y -axis) for 100 rung-ladder in the doped D-Mott phase and edge current $0.0001t$ ($U = 0.25$, $t = V_{\perp} = 1$, $J_{\perp} = 1.7$, and doping $\delta = 0.04$). Top and bottom densities coincide. Note that for these model parameters there is SF/DDW order at half-filling (see Fig. 2(a)); the phase boundary between the D-Mott and SF/DDW phase moves downwards when the system is doped.

well-converged results, it is crucial to apply several runs (sweeps) of the finite-system DMRG algorithm until convergence is observed numerically. We have typically performed of the order of 10 to 20 sweeps and observed convergence after typically 5 to 7 sweeps.

Up to 800 states were kept for DMRG runs; following standard practice, the number of states kept was initially chosen to be much smaller and increased during sweeps. For systems up to about 100 rungs, final results were independent of the way the number of states was augmented. For systems well beyond 100 rungs we have observed that in the SF/DDW phase, DMRG runs that started with a very low number of states kept, converged to a result where the current amplitudes were somewhat suppressed with respect to runs that started with high precision and yielded results in perfect agreement with those found for shorter systems. The low precision calculation introduces a phase slip π at the center (Fig. 12).

Do we really have true long-range order in the orbital currents? If there is not true long-range order, one might speculate that the introduction of a phase slip (of the type seen in Fig. 12) at low energetic cost is the way how long-ranged correlations are lost in this system. However, we did not observe, for systems up to 200 rungs, any significant decrease of the magnitude of the triggered current pattern. Considering Fig. 13, one actually sees that maximum current amplitudes grow from system size 50 to 100, in line with the SF/DDW suppression by edges reported above, to stay constant after that. One

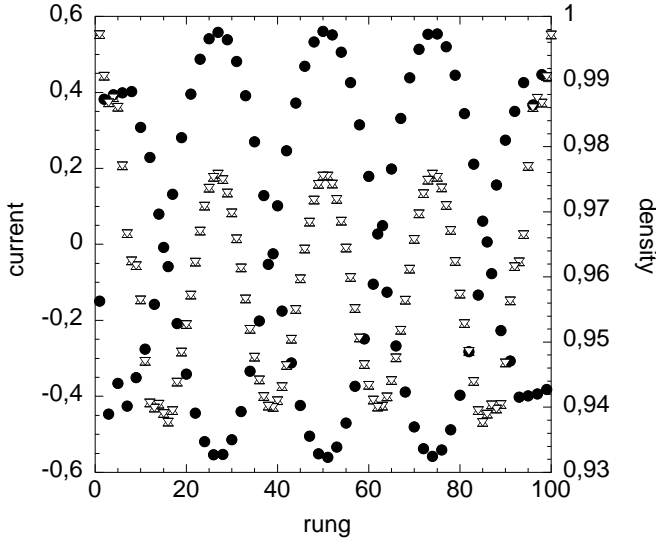


FIG. 10: Rung current (solid circles, left y -axis, units of t) and electronic densities on top and bottom ladder leg (up and down triangles, right y -axis) for 100 rung-ladder in the SF/DDW phase and edge current $0.0001t$ ($U = 0.25$, $t = V_{\perp} = 1$, $J_{\perp} = 1.5$, and doping $\delta = 0.04$). Top and bottom densities coincide.

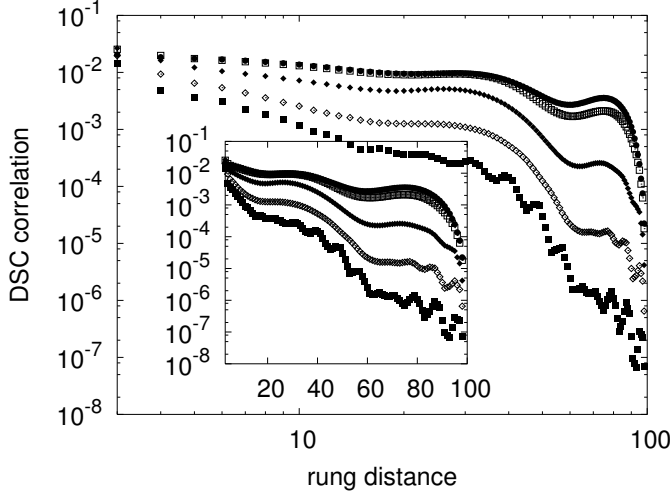


FIG. 11: Log-log plot of DSC correlations for a 100-rung ladder with $U = 0.25$, $t = V_{\perp} = 1$ and doping $\delta = 0.04$, for different values of J_{\perp} (from bottom to top): 1.3 (solid squares), 1.5 (open diamonds), 1.7 (solid diamonds), 2.0 (open squares), and 2.6 (solid circles). The first two values are in the SF/DDW phase, the last three in the doped D-Mott phase. The inset shows a lin-log plot of the same data.

might envisage that the open boundary conditions lock in the currents, leaving us with seeming long-ranged order. The repeated observation that open boundary conditions seem to disfavor SF/DDW does not support this point of view. It might also be speculated that our filling factors, 4, 8 and 12 percent away from half-filling, allow the formation of commensurate current patterns which may

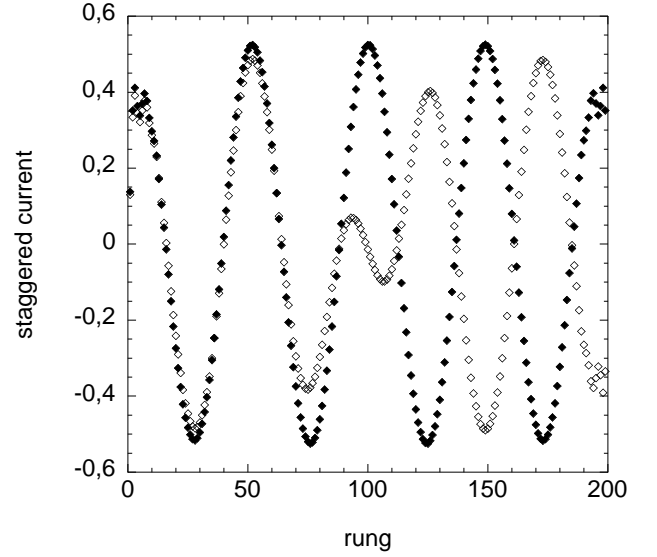


FIG. 12: Staggered rung current for 200 rung-ladder in the SF/DDW phase and edge current $0.0001t$ ($U = 0.25$, $t = V_{\perp} = 1$, $J_{\perp} = 1.5$, and doping $\delta = 0.04$). Final number of states $m = 400$ was reached starting from $m = 100$ (open diamonds) and $m = 400$ (solid diamonds).

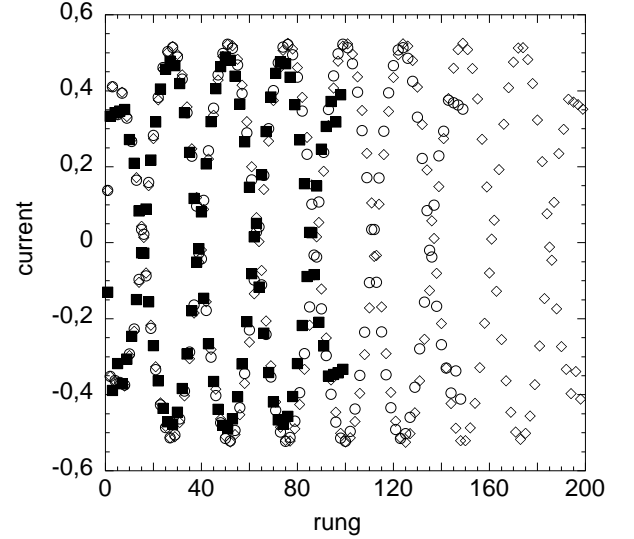


FIG. 13: Rung current in the SF/DDW phase and edge current $0.0001t$ ($U = 0.25$, $t = V_{\perp} = 1$, $J_{\perp} = 1.5$, and doping $\delta = 0.04$) for ladder lengths 100 (solid squares), 150 (circles), 200 (diamonds).

show long-ranged order as opposed to the generic case of incommensurate filling. Introducing 11 holes on a 192 rung ladder to model an approximation to a generic incommensurate filling on a finite system, however, we do not observe current decay either (Fig. 14).

The SF/DDW phase survives up to quite substantial dopings away from half-filling. Fig. 15 shows current and density oscillations in the SF/DDW phase of a 200-rung ladder for doping $\delta = 0.08$. For the parameter sets stud-

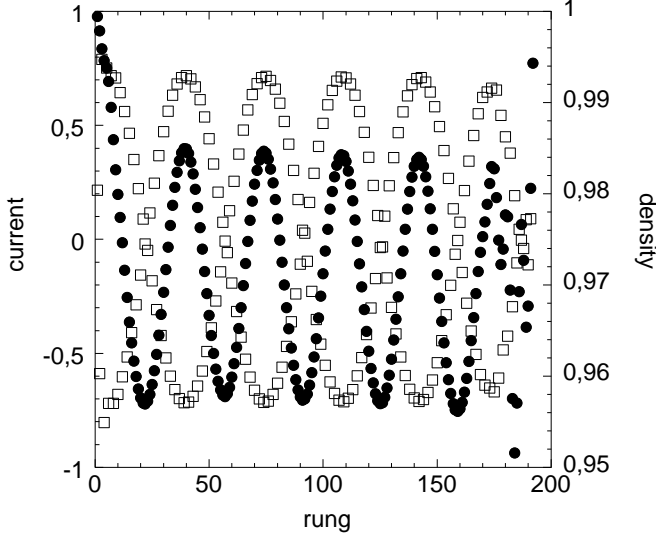


FIG. 14: Rung current (open squares, left y -axis, units of t) and electronic densities (solid circles, right y -axis) for 192-rung ladder in the SF/DDW phase ($U = -0.4$, $t = 1$, $V_{\perp} = 0.9$, $J_{\perp} = 2$), edge current $0.0001t$ and 11 holes (i.e., $\delta \approx 0.0286$, $1/\delta \approx 34.9$). The disturbed density pattern and slight current reduction on the far end of the ladder is due to the presence to one unpaired hole.

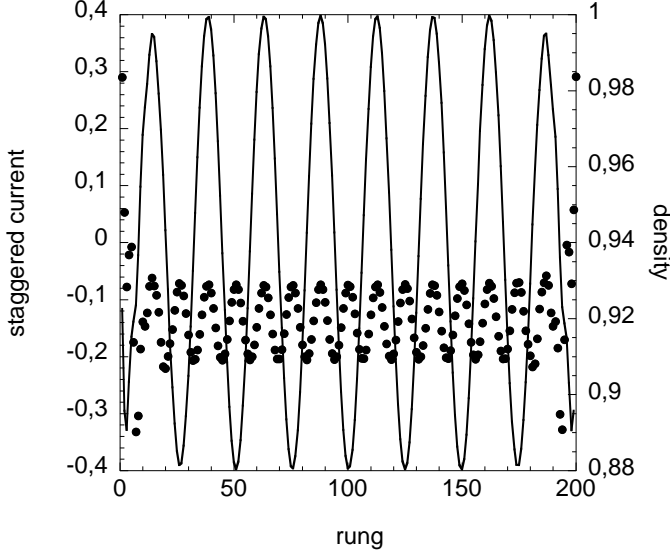


FIG. 15: Rung current (lines, left y -axis, units of t) and electronic densities (solid circles, right y -axis) for 200-rung rung-ladder in the SF/DDW phase for $\delta = 0.08$ and edge current $0.0001t$ ($U = 0.25$, $t = V_{\perp} = 1$, $J_{\perp} = 1.5$).

ied, the phase transition where SF/DDW order is finally suppressed to zero seems to occur roughly between 10 and 20 percent doping; a more precise estimate would require a more systematic study of the doping dependence of the SF/DDW phase as a function of the interaction parameters.

V. EFFECTIVE FIELD THEORY DESCRIPTION OF THE DOPED LADDER

In this section we try to understand the DMRG results in Sec. IV using weak-coupling RG/bosonization arguments. We will be particularly interested in what these arguments predict regarding the possibility of having true long-range order for the considered doping levels.

A. Physical observables

We first present the set of relevant physical observables and their bosonized expressions for the case of an arbitrary filling for which the Fermi energy crosses both bands. This includes the half-filled case discussed in Sec. III, as well as the doping levels studied numerically in Sec. IV.

The rung current operator is

$$j_{\perp}(x) = j_{2k_F} [\cos(2k_F x + \phi_{+\rho}) \cos \phi_{+\sigma} \cos \theta_{-\rho} \cos \theta_{-\sigma} + \sin(2k_F x + \phi_{+\rho}) \sin \phi_{+\sigma} \sin \theta_{-\rho} \sin \theta_{-\sigma}]. \quad (5.1)$$

Furthermore, the density operator $n_{\ell}(x)$ on leg ℓ is

$$n_{t,b}(x) = (1 - \delta) + \frac{1}{\pi} \frac{\partial \phi_{+\rho}}{\partial x} \pm n_{2k_F} [\cos(2k_F x + \phi_{+\rho}) \cos \phi_{+\sigma} \sin \theta_{-\rho} \cos \theta_{-\sigma} - \sin(2k_F x + \phi_{+\rho}) \sin \phi_{+\sigma} \cos \theta_{-\rho} \sin \theta_{-\sigma}] + n_{4k_F} \cos(4k_F x + 2\phi_{+\rho}) \cos 2\phi_{+\sigma}. \quad (5.2)$$

The quantity $2k_F$ was defined in Eq. (4.5). The nonuniversal coefficients j_{2k_F} , n_{2k_F} and n_{4k_F} depend on the short-distance cutoff of the theory.

The $4k_F$ term in $n_{\ell}(x)$ should be particularly noted. It does not come out of a naive calculation of the density operator using the bosonization formula (3.7); however, a more general, phenomenological reasoning shows that such higher harmonics terms are generally expected.^{65,74} The form of the $4k_F$ term in $n_{\ell}(x)$ was deduced by White *et al.*⁴⁵ They considered the $4k_F$ term in the correlation function for the *square* of the density operator, as resulting from the product of the $2k_F$ terms in the density operator calculated from the bosonization formula, and then (implicitly) argued that a similar $4k_F$ contribution to that correlation function would be expected to come from the product of the constant term and a $4k_F$ term in the density operator. Higher harmonics than $2k_F$ in $j_{\perp}(x)$ and $4k_F$ in $n_{\ell}(x)$ have been neglected in the expressions above as they are expected to give at most only minor quantitative corrections to the terms already included.

The density operator above is more complicated than the one discussed for the half-filled CDW phase in Sec. III D. It is therefore instructive to see how the expectation value of $n_{\ell}(x)$ reduces to the correct form at half-filling. In that case, both $\phi_{+\rho}$ and $\phi_{+\sigma}$ are locked in all four phases (see Table I). This gives $\langle \partial_x \phi_{+\rho} \rangle = 0$

and $\langle \cos 2\phi_{+\sigma} \rangle \neq 0$; furthermore, from $4k_F = 2\pi$ it follows that $\langle \cos(4k_F x + 2\phi_{+\rho}) \rangle = \langle \cos 2\phi_{+\rho} \rangle \neq 0$. Thus the expectation value of the $4k_F$ term is independent of x at half-filling. Consequently, the only way to obtain the correct average density of one electron per site is to have $n_{4k_F} \equiv 0$ in this case. Hence the expectation value of the deviation of the density from its average value, $\delta n_\ell(x) \equiv n_\ell(x) - 1$, reduces to the expectation value of the $2k_F$ term, which is only nonzero in the CDW phase, in agreement with the simplified discussion of the density operator in Sec. III D.

Finally, we note that since the DSC and SSC operators have zero momentum, their bosonized expressions are the same as at half-filling; see Eqs. (3.18)-(3.20). (We will not consider SSC order in the following, since the doped S-Mott phase was not studied in Sec. IV.)

B. True long-range order scenario

It was argued in Sec. IV that the DMRG results are consistent with true long-range orbital current and charge density wave order. From the bosonization point of view, to have true long-range order it is necessary that certain bosonic fields become locked to appropriate values. In this subsection we show that if this locking occurs, the resulting expectation values and correlation functions of the physical observables of interest, as calculated from the bosonized expressions in Sec. V A, are in good qualitative agreement with the DMRG results. The assumption that the locking occurs is easily justified for all bosonic fields in question except the symmetric charge field $\phi_{+\rho}$. The conditions for locking this field will be investigated in detail in Sec. V C.

Let us first consider the SF/DDW phase. True long-range order in the currents, $\langle j_\perp(x) \rangle \neq 0$, requires that the four fields $\phi_{+\rho}$, $\phi_{+\sigma}$, $\theta_{-\rho}$, and $\theta_{-\sigma}$ become locked to appropriate values as determined by Eq. (5.1). The momentum-conserving interaction (3.13), which contains cosines of the three latter fields, is present also away from half-filling, and weak-coupling one-loop RG calculations^{31,32,37,59} show that it can cause $\phi_{+\sigma}$, $\theta_{-\rho}$, and $\theta_{-\sigma}$ (or $\phi_{-\sigma}$) to lock also in the doped case, at least if the doping is not too large. This picture is expected to hold also for stronger interactions. Let us now assume that also the symmetric charge field $\phi_{+\rho}$ can become locked for the dopings considered in Sec. IV. There is then a finite energy gap to excitations in $\phi_{+\rho}$. Using the field-locking pattern for $\phi_{+\sigma}$, $\theta_{-\rho}$, and $\theta_{-\sigma}$ in Table I, and evaluating the expectation value of the current operator semiclassically,⁷⁵ we find

$$\langle j_\perp(x) \rangle \approx j_0 \cos(2k_F x + \langle \phi_{+\rho} \rangle), \quad (5.3)$$

with $j_0 = j_{2k_F} \langle \cos \phi_{+\sigma} \cos \theta_{-\rho} \cos \theta_{-\sigma} \rangle \neq 0$. Since $\phi_{+\rho}$ and $\phi_{+\sigma}$ are locked, we also have (with $n_t(x) = n_b(x) \equiv n(x)$ in the SF/DDW phase)

$$\langle n(x) \rangle = (1 - \delta) + n_0 \cos(4k_F x + 2\langle \phi_{+\rho} \rangle), \quad (5.4)$$

with $n_0 = n_{4k_F} \langle \cos 2\phi_{+\sigma} \rangle \neq 0$. This shows that $(2k_F, \pi)$ -SF/DDW order and $(4k_F, 0)$ -CDW order coexist in the SF/DDW phase. Furthermore, if the non-universal coefficient n_{4k_F} is positive, the minima of the electron density always occur at the zeros (anti-phase domain walls) of the current. These results are in agreement with the findings in Sec. IV. The different solutions for $\langle \phi_{+\rho} \rangle$ give rise to degenerate ground states which are related to each other by translations by a lattice vector (in the DMRG calculations, this degeneracy is of course lifted by the open boundary conditions, leaving only a two-fold degeneracy due to the breaking of time reversal symmetry). Fig. 16 shows a fit of these analytical results for the SF/DDW phase to the DMRG results for two different dopings. The agreement is quite good. If the true long-range order scenario is in fact realized, we expect that the minor differences between the numerical and analytical results could be removed, at least in principle, by improving the latter by taking into account boundary and finite-size effects, corrections due to the presence of higher harmonics, and by going beyond the semiclassical approximations used in evaluating the expectation values.

By using similar arguments as for the SF/DDW phase, one also predicts, again in agreement with DMRG results, that there is coexistence of $(2k_F, \pi)$ -CDW and $(4k_F, 0)$ -CDW order in the CDW phase, while in the doped D-Mott phase there is “only” $(4k_F, 0)$ -CDW order. The reason for the ubiquity of $(4k_F, 0)$ -CDW order is that this order parameter only contains the fields $\phi_{+\rho}$ and $\phi_{+\sigma}$, both of which are locked in all phases in this true long-range order scenario.

This scenario furthermore predicts that the asymptotic decay of DSC correlations is exponential in all phases. The DSC correlation length is expected to be smallest in the CDW phase because then the field-locking differs from what the DSC operator wants in both the $-\rho$, $-\sigma$, and $+\rho$ sectors. In the SF/DDW phase the correlation length should be larger because there is no longer disagreement in the $-\rho$ sector. In the doped D-Mott phase the correlation length is larger still because the $-\sigma$ sector also matches up, the only exponential decay left coming from the $+\rho$ sector. These predictions for the qualitative behavior of the DSC correlations are in good agreement with the DMRG results (with the qualifier that in the case of the doped D-Mott phase, the nature of the asymptotic decay of DSC correlations is difficult to deduce from the DMRG data; see the discussion in Sec. IV).

C. True long-range order and Umklapp interactions

The crucial assumption which enabled the true long-range order scenario just discussed to emerge from the bosonization formulas was that the symmetric charge field $\phi_{+\rho}$ can become locked for the dopings and interaction parameters considered in Sec. IV. In this subsection we use symmetry arguments to derive the form of

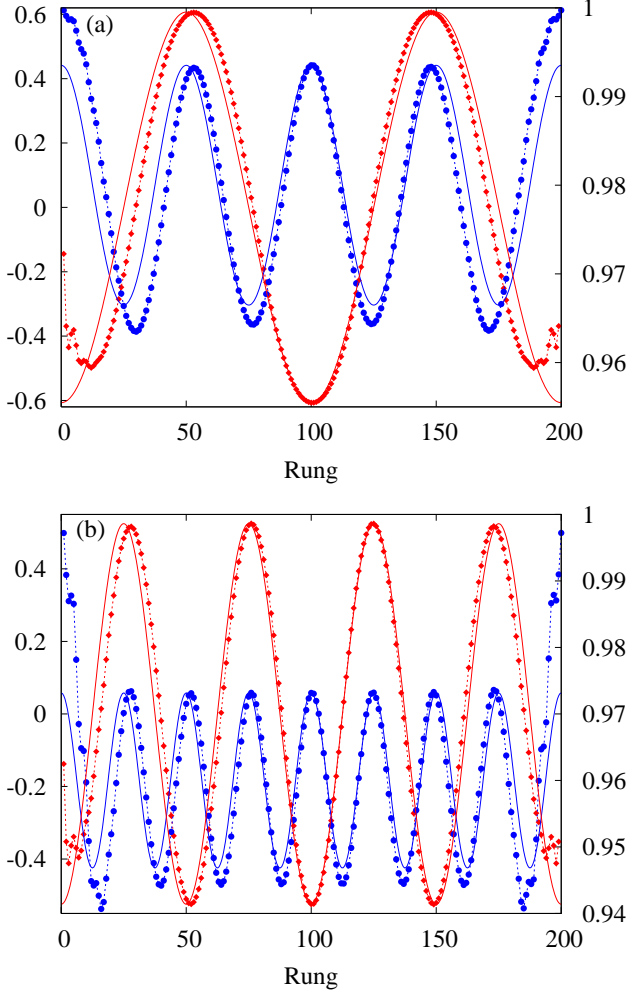


FIG. 16: (Color online) (a) Staggered rung current $j_s(x)$ (red curves, left y-axis) and electron density per site $n(x)$ (blue curves, right y-axis) as a function of rung index x in the SF/DDW phase of a 200-rung ladder with $\delta = 0.02$. Shown are DMRG results (diamonds and circles for currents and densities, respectively, connected by dashed lines to guide the eye) and analytical fits from the true long-range order scenario (full lines). The model parameters for the DMRG calculation are $t = V_\perp = 1$, $U = 0.25$, $J_\perp = 1.5$ and $J_\parallel = V_\parallel = 0$. The values of the fitting parameters are $|j_0| \approx 0.61$ and $n_0 \approx 0.0135$. (b) Plots for the same model parameters as above, except that the doping $\delta = 0.04$ and the values of the fitting parameters are $|j_0| \approx 0.52$ and $n_0 \approx 0.0132$.

the terms that, under the right circumstances, are able to lock $\phi_{+\rho}$. It will be shown that these terms are Umklapp interactions, and that they are allowed by symmetry in the low-energy effective Hamiltonian only when the average number of electrons per site, n , is a rational number p/q . The further analysis suggests that the Umklapp interactions are only able to lock $\phi_{+\rho}$ for relatively small values of q . Therefore this weak-coupling RG/bosonization analysis appears not to support a true long-range order scenario for the dopings considered in

Sec. IV, which correspond to quite large (≥ 25) values of q .

If the low-energy effective Hamiltonian, denoted by H_{eff} , is invariant under global translations in $\phi_{+\rho}$,

$$\phi_{+\rho}(x) \rightarrow \phi_{+\rho}(x) + \alpha \quad (\alpha \text{ arbitrary real}), \quad (5.5)$$

locking $\phi_{+\rho}$ implies that this continuous symmetry must be spontaneously broken, which is impossible in one dimension. Therefore, to lock $\phi_{+\rho}$ it is necessary that there be terms in H_{eff} that break this continuous symmetry. Furthermore, the Hamiltonian can only contain gauge-invariant terms. The bosonic fields themselves are not gauge-invariant, only derivatives and exponentials of them are. Of these, only exponentials of $\phi_{+\rho}$ are not invariant under (5.5), as they break the continuous symmetry down to a discrete one. Thus one is led to consider terms of the form

$$H_Q = F_Q + F_Q^\dagger, \quad F_Q \equiv \int dx A_Q(x) e^{iQ\phi_{+\rho}(x)}, \quad (5.6)$$

where $Q \neq 0$ and $A_Q(x)$ is an operator that we define to be invariant under (5.5). We may take $Q > 0$ without loss of generality.

We will use the fact that H_Q must be invariant under certain symmetry operations (reflections and translations in real space) to deduce under what conditions H_Q can appear in H_{eff} , and what the allowed values of Q are in that case. However, to do this it turns out that we will also need to know how H_Q transforms under translations in $\phi_{-\rho}$. Since the conjugate field $\theta_{-\rho}$ is locked in all phases, $\phi_{-\rho}$ is disordered, so that an operator containing terms with exponentials of $\phi_{-\rho}$ will be irrelevant in the RG sense. Thus, if H_Q is to have a chance of causing true long-range order, we must assume that $A_Q(x)$ does not contain such terms, which implies that H_Q is invariant under global continuous translations in $\phi_{-\rho}$,

$$\phi_{-\rho} \rightarrow \phi_{-\rho} + \beta \quad (\beta \text{ arbitrary real}). \quad (5.7)$$

Let us first consider reflection symmetry. H_Q must be invariant under the transformation

$$c_{t,x,s} \rightarrow c_{b,x,s}, \quad c_{b,x,s} \rightarrow c_{t,x,s} \quad (5.8)$$

which interchanges the “top” and “bottom” leg. By regarding the two sites on a rung as forming a one-dimensional lattice in the transverse (y) direction with periodic boundary conditions, we see that (5.8) is a translation by one lattice spacing in this two-site lattice, and is therefore effected by the unitary operator $e^{-i\mathcal{P}_y}$ where \mathcal{P}_y is the momentum operator in the y direction. The allowed transverse momenta are $k_y = 0$ and π , associated with the bonding and antibonding bands 2 and 1, respectively. Thus

$$\mathcal{P}_y = \pi \sum_{x,s} c_{1xs}^\dagger c_{1xs} = \pi \sum_{P,s} \mathcal{N}_{P1s}. \quad (5.9)$$

One finds that $e^{-i\mathcal{P}_y}$ transforms the continuum field operators as

$$\psi_{P1s}(x) \rightarrow -\psi_{P1s}(x), \quad \psi_{P2s}(x) \rightarrow \psi_{P2s}(x). \quad (5.10)$$

Thus the symmetry under leg interchange implies that any term in the Hamiltonian must contain an even number of both 1- and 2-operators of this type (the latter due to conservation of the total number of particles). Bosonization gives $\mathcal{P}_y = \int dx (\partial_x \phi_{+\rho} - \partial_x \phi_{-\rho})$ which shows that $e^{-i\mathcal{P}_y}$ generates translations in $\theta_{\pm\rho}$. We would however like to find an operator that transforms the field operators like (5.10) while at the same time generating translations in $\phi_{\pm\rho}$, as that would give information about Q . Such an operator is $e^{-i\mathcal{R}}$, where \mathcal{R} is obtained by modifying \mathcal{P}_y in (5.9) by a factor of P , which changes $\phi \rightarrow \theta$ in the bosonic representation:

$$\mathcal{R} = \pi \sum_{P,s} P \mathcal{N}_{P1s} = \int dx (\partial_x \theta_{+\rho} - \partial_x \theta_{-\rho}). \quad (5.11)$$

As desired, $e^{-i\mathcal{R}}$ leaves all bosonic fields invariant except $\phi_{\pm\rho}$ which transform as

$$\phi_{-\rho} \rightarrow \phi_{-\rho} - \pi, \quad \phi_{+\rho} \rightarrow \phi_{+\rho} + \pi. \quad (5.12)$$

Thus invariance of H_Q under this transformation implies, when we use that H_Q must be invariant under (5.7) separately, that Q must be an even integer.

Next, consider translation symmetry.⁷⁶ H_Q must be invariant under the transformation

$$c_{\ell,x,s} \rightarrow c_{\ell,x+1,s} \quad (5.13)$$

which translates the system by one lattice spacing in the x direction. This transformation is generated by the operator $e^{-i\mathcal{P}_x}$ where \mathcal{P}_x is the momentum operator in the x direction, given by

$$\begin{aligned} \mathcal{P}_x &= \sum_{k\lambda s} k n_{k\lambda s} \approx \sum_{P\lambda s} P k_{F\lambda} \mathcal{N}_{P\lambda s} \\ &= \frac{1}{\pi} \int dx \left[(k_{F1} + k_{F2}) \partial_x \theta_{+\rho} + (k_{F2} - k_{F1}) \partial_x \theta_{-\rho} \right] \end{aligned} \quad (5.14)$$

Clearly $e^{-i\mathcal{P}_x}$ leaves all bosonic fields unchanged except $\phi_{\pm\rho}$ which transform as

$$\phi_{-\rho} \rightarrow \phi_{-\rho} - k_{F1} + k_{F2}, \quad (5.15)$$

$$\phi_{+\rho} \rightarrow \phi_{+\rho} + k_{F1} + k_{F2} = \phi_{+\rho} + \pi n, \quad (5.16)$$

where we used (4.5) to express (5.16) in terms of the average number of electrons per site, n . Again invoking the invariance of H_Q under (5.7), it follows that (5.16) requires Qn to be an even integer. This is impossible if n is an irrational number, implying that H_Q is not allowed in H_{eff} in this case. Therefore true long-range order is excluded for incommensurate fillings. If instead n is rational, i.e.,

$$n = p/q \quad (5.17)$$

where p and q are coprimes (i.e., integers with no common divisors), the values of Q that make both Q and Qn even integers are

$$Q = 2rq, \quad r = 1, 2, \dots \quad (5.18)$$

Therefore the terms H_{2rq} are allowed in H_{eff} in this case.

We now consider the physical interpretation of these terms. As they are not invariant under (5.5), they do not commute with the generator of these translations, given by $G_{\phi_{+\rho}} = \int dx \Pi_{\phi_{+\rho}} = (\mathcal{N}_L - \mathcal{N}_R)/2$, where $\Pi_{\phi_{+\rho}} = -\partial_x \theta_{+\rho}/\pi$ is the conjugate momentum of $\phi_{+\rho}$, and

$$\mathcal{N}_P \equiv \sum_{\lambda s} \mathcal{N}_{P\lambda s} = \frac{1}{\pi} \int dx \partial_x (\phi_{+\rho} + P\theta_{+\rho}) \quad (5.19)$$

is the number operator for right-/left-moving electrons. Because $A_{2rq}(x)$ is invariant under independent global continuous translations of $\phi_{+\rho}$ and $\theta_{+\rho}$ (the latter due to conservation of total particle number), we have $[\mathcal{N}_P, A_{2rq}(x)] = 0$. This gives

$$[\mathcal{N}_P, F_{2rq}] = -2rqP F_{2rq}, \quad (5.20)$$

which shows that F_{2rq} and F_{2rq}^\dagger are raising/lowering operators (by $2rq$ quanta) for \mathcal{N}_P : F_{2rq} scatters $2rq$ electrons from right to left while F_{2rq}^\dagger scatters them the other way. Furthermore, the commutator

$$[\mathcal{P}_x, F_{2rq}] = -4k_F r q F_{2rq} \quad (5.21)$$

shows that the associated momentum transfer is $\mp 4k_F r q$ for F_{2rq} and F_{2rq}^\dagger , respectively, which reduces to $\mp 2\pi r p$ for $n = p/q$. Thus H_{2rq} is an Umklapp interaction. Note that the invariance of H_Q under (5.7) was used in the derivation of (5.21).

Of all the Umklapp interactions H_{2rq} , $r = 1, 2, \dots$, that are allowed in H_{eff} for commensurate density $n = p/q$, the operator H_{2q} corresponding to $r = 1$ is most relevant in the RG sense, and is therefore the one we will focus on in the rest of the discussion. H_{2q} scatters $2q$ electrons from the left to the right side of the Fermi surface (and vice versa), with associated momentum transfer $\pm 2\pi p$.⁷⁷ The interaction H_{2q} with $q = 1$ (which is allowed in H_{eff} at half-filling) will be referred to as the basic-Umklapp interaction. The interactions H_{2q} with $q > 1$ will be referred to as multiple-Umklapp interactions.

The derivation presented here shows that when the density n is moved away from the commensurate value p/q , the term H_{2q} is no longer allowed in H_{eff} . Another way of understanding this is from the fact that when n moves away from p/q , $A_{2q}(x)$ acquires factors that oscillate in space (this is intimately related to the fact that the momentum $4k_F q$ transferred by H_{2q} now deviates from the reciprocal lattice vector $2\pi p$), and these make H_{2q} average to zero on sufficiently long length scales, thereby rendering it an irrelevant operator. For example, for doping δ away from half-filling the basic-Umklapp interaction is proportional to $\cos(2\phi_{+\rho} + 4k_F x) = \cos(2\phi_{+\rho} + 2\pi\delta x)$.

Thus the cosine oscillates with x and averages to zero over length scales much bigger than $1/\delta$.

Since the $-\rho$ and $\pm\sigma$ sectors are gapped out, the parts of the Hamiltonian containing fields belonging to these sectors can be replaced by their expectation values. The low-energy effective Hamiltonian is then described in terms of the fields in the remaining $+\rho$ sector. H_{eff} has a quadratic part given by the Luttinger liquid Hamiltonian⁷⁸

$$H_{\text{LL}} = \int dx \frac{v_{+\rho}}{2\pi} \left[K_{+\rho} (\partial_x \theta_{+\rho})^2 + \frac{1}{K_{+\rho}} (\partial_x \phi_{+\rho})^2 \right], \quad (5.22)$$

where $v_{+\rho}$ and $K_{+\rho}$ are the effective velocity and Luttinger parameters, respectively. H_{LL} describes a critical (Luttinger liquid) fixed point with gapless excitations in $\phi_{+\rho}$. For commensurate density $n = p/q$, H_{eff} will also contain H_{2q} if the latter is a relevant operator with respect to H_{LL} . In that case H_{2q} will lock $\phi_{+\rho}$ in one of the minima of its potential, thereby opening up a gap in $\phi_{+\rho}$, causing true long-range order. Assuming that $\langle A_{2q}(x) \rangle \neq 0$ for the field-locking pattern in the gapped sectors (if $\langle A_{2q}(x) \rangle$ should happen to vanish, true long-range order is ruled out), the only decay of the two-point function of $H_{2q} \equiv \int dx \mathcal{H}_{2q}(x)$ comes from the $\exp(\pm 2iq\phi_{+\rho})$ factors, giving the asymptotic decay $\langle \mathcal{H}_{2q}(x) \mathcal{H}_{2q}(0) \rangle \sim |x|^{-2d_{2q}}$, where

$$d_{2q} = q^2 K_{+\rho} \quad (5.23)$$

is the scaling dimension of H_{2q} . If $d_{2q} < 2$, H_{2q} is perturbatively relevant. Thus the critical value of $K_{+\rho}$ below which H_{2q} is expected to open up a gap and cause true long-range order is from this simple argument estimated to be

$$K_{+\rho}^c \equiv 2/q^2. \quad (5.24)$$

The dopings considered in Sec. IV correspond to very large values of q , and consequently very small values of $K_{+\rho}^c$ (see Table II). For weak repulsive interactions $K_{+\rho}$ is expected to be slightly less than 1 ($K_{+\rho} = 1$ in the noninteracting model). Therefore H_{2q} is strongly irrelevant for weak interactions in the doped ladder, and consequently true long-range order is not possible in that case. For larger interactions a definite statement can no longer be made, as $K_{+\rho}$ is not known as a function of U , V_{\perp} , J_{\perp} etc. On the other hand, true long-range order would certainly be very surprising. Although one generally expects $K_{+\rho}$ to decrease with increasing interaction strength, the values of $K_{+\rho}^c$ for the nonzero dopings in Table II are, to the best of our knowledge, orders of magnitude smaller than the smallest known values of $K_{+\rho}$ in the t - J and Hubbard ladders,⁷⁹ which furthermore are obtained only for very strong interactions, much stronger than the ones used in Sec. IV. Correspondingly, only for low commensurabilities (i.e., small values of q) has it been found that $K_{+\rho}$ can become as small as $K_{+\rho}^c$ for sufficiently strong interactions in theoretical ladder models, with true long-range order as a result.

δ (%)	p	q	$K_{+\rho}^c$
0	1	1	2
2	49	50	0.0008
2.86	373	384	0.0000136
4, 8, 12	24, 23, 22	25	0.0032

TABLE II: The parameters p , q , and $K_{+\rho}^c = 2/q^2$ evaluated for the rational dopings $\delta = 1 - p/q$ considered in Sec. IV. The values of these parameters at half-filling are shown for comparison.

We end this subsection with some remarks on how the discussion presented here relates to previous work. It is already known in the literature that RG/bosonization arguments predict that having true long-range order in the two-leg ladder requires relevant Umklapp interactions and that Umklapp interactions are usually irrelevant away from half-filling. These conclusions, and arguments leading to them, have been invoked either explicitly or implicitly in many previous studies of interacting electrons on a two-leg ladder (see, e.g., Refs. 31,32,33,35,37,38,45,46,58,59,60,63,65,80). The discussion given here based on symmetry considerations, which is a generalization to the two-leg ladder of previous discussions for a single chain,^{76,81,82} allowed for a more systematic and general derivation of these results. In particular, the derivation of Eq. (5.23) enabled us to give a semi-quantitative discussion of the question of *how* irrelevant (or relevant) the most relevant allowed Umklapp operator is for an arbitrary rational filling.

D. Quasi long-range order scenario

The weak-coupling analysis in the previous subsection suggests that Umklapp interactions are unlikely to be relevant for the dopings considered in Sec. IV, and that as a consequence the effective theory at sufficiently low energies and long wavelengths is given by the Luttinger liquid Hamiltonian in Eq. (5.22), with gapless excitations in $\phi_{+\rho}$. This will be referred to as the quasi long-range order scenario, as it implies that for sufficiently large distances correlation functions of exponentials of $\phi_{+\rho}$ decay as power laws with $K_{+\rho}$ -dependent exponents (the same features hold for $\theta_{+\rho}$). In this subsection we summarize some consequences of this scenario, both for infinite and finite ladders. From a numerical comparison with the Luttinger-liquid predictions for finite ladders, we find that the DMRG results are not consistent with the quasi long-range order scenario. This analysis complements the discussions in Secs. IV and VB which concluded that the DMRG results are consistent with a true long-range order scenario.

We start by summarizing the Luttinger-liquid predictions for the correlation functions for the charge density, orbital current and DSC pairing operators in the doped

Correlation function	Phase					
	SF/DDW		CDW		Doped D-Mott	
$(2k_F, \pi)$ -SF/DDW	$K_{+\rho}/2^{37}$	(const)	exp	(exp)	exp	(exp)
$(2k_F, \pi)$ -CDW	exp	(exp)	$K_{+\rho}/2^{37}$	(const)	exp	(exp)
DSC	exp	(exp)	exp	(exp)	$1/(2K_{+\rho})^{31,37,45,80}$	(exp)
$(4k_F, 0)$ -CDW	$2K_{+\rho}$	(const)	$2K_{+\rho}$	(const)	$2K_{+\rho}^{31,45,80}$	(const)

TABLE III: Bosonization predictions for the asymptotic decay of two-point correlation functions in the two-leg ladder. In each cell, the first entry is the decay when $\phi_{+\rho}$ is gapless (quasi long-range order scenario); the second entry (in parenthesis) is the decay when $\phi_{+\rho}$ is gapped (true long-range order scenario). Power-law decay is indicated by the decay exponent, ‘const’ means no decay, and ‘exp’ means exponential decay.

SF/DDW, CDW and D-Mott phases in an infinitely long ladder. The nature of the decay of these correlation functions is easily obtained from the bosonized expressions in Sec. V A, the field-locking patterns for the $\pm\sigma$ and $-\rho$ sectors (Table I), and the correlation functions of exponentials of $\phi_{+\rho}$ and $\theta_{+\rho}$. The results are summarized in Table III. A few remarks are in order. The $4k_F$ density correlations show the same qualitative behavior across the entire phase diagram. In the SF/DDW and CDW phases, the SF/DDW and $2k_F$ -CDW correlations, respectively, dominate over the $4k_F$ -CDW correlations. In the doped D-Mott phase, the DSC correlations are dominant for $K_{+\rho} > 1/2$ while the $4k_F$ -CDW correlations dominate for $K_{+\rho} < 1/2$.^{31,45,80} Schulz⁸⁰ has argued that $K_{+\rho} \rightarrow 1$ as $\delta \rightarrow 0^+$ in the doped D-Mott phase. Therefore one expects DSC correlations to be dominant in the doped D-Mott phase sufficiently close to half-filling. (For easy comparison the nature of the asymptotic decay when $\phi_{+\rho}$ is gapped has been indicated in parenthesis in Table III. The cases we have commented on here are those for which the true and quasi long-range order scenarios predict qualitatively different decays.)

The expressions for the power-law exponents in Table III spur the question of whether the doped ladder might be described by a quasi long-range order scenario with a very small $K_{+\rho}$. Unfortunately, the strong finite-size effects in the DMRG results severely complicate a comparison with the Luttinger-liquid predictions for an infinite ladder. It is much preferred to compare the DMRG results with analytical predictions for a ladder of *finite* size and with *open* boundary conditions. White *et al.*⁴⁵ have recently discussed such a ladder that is in a Luttinger-liquid phase of the type described above, i.e., in which the low-energy effective theory is given by the gapless Luttinger-liquid Hamiltonian H_{LL} in the $+\rho$ sector and the three other sectors are gapped. It was shown that in such a system the boundaries will act as impurities and induce generalized Friedel oscillations in the charge density which decay away from the boundaries. These Friedel oscillations have fundamental wavevector $4k_F$ and thus period $1/\delta$. White *et al.* furthermore showed that the density amplitude in the middle of the ladder should scale with the ladder length L as $L^{-K_{+\rho}}$. To investigate whether the $4k_F$ charge density oscillations found in Sec.

IV might be interpreted as generalized Friedel oscillations in such a Luttinger liquid, one can plot the mid-ladder density amplitude as a function of the ladder length in a log-log plot and try to fit the results to a straight line; from its slope one can extract a value for $K_{+\rho}$.⁴⁵

We have attempted this kind of fit of the DMRG results for two different cases, both at 4 percent doping: In the SF/DDW phase ($t = V_{\perp} = 1$, $U = 0.25$ and $J_{\perp} = 1.5$), and in the doped D-Mott phase (same parameters except $J_{\perp} = 1.8$). In both cases the mid-ladder density amplitude is found not to decay with ladder length for sufficiently large ladders, so that the fit gives $K_{+\rho} = 0$. This result does not support an interpretation of the density oscillations as generalized Friedel oscillations in a Luttinger liquid; instead it is consistent with a true long-range order scenario. Even if one were to take into account corrections to H_{LL} due to irrelevant operators (such as the basic-Umklapp interaction discussed more below), one would still expect that the mid-ladder density amplitude should decrease monotonically towards zero with increasing ladder length, instead of approaching a nonzero constant. Thus if the DMRG results reflect the true behavior of the system the quasi long-range order scenario appears to be ruled out.

E. Neglecting quantum fluctuations: A classical description of the doped ladder

The fact that the basic-Umklapp interaction is relevant in the half-filled ladder enabled true long-range order in that case. The analysis in Sec. V C suggests that in the doped ladder the basic-Umklapp interaction is irrelevant: although it can cause significant ordering tendencies on length scales $\lesssim O(1/\delta)$, it can be neglected on length scales $\gg 1/\delta$.⁸³ The Luttinger-liquid behavior discussed in Sec. V D, with quasi long-range ordered correlation functions, would thus be expected to manifest itself in this asymptotic regime.³⁷ One would think that this regime should be accessible numerically since the dopings considered in Sec. IV correspond to values of $1/\delta$ that are considerably smaller than the largest system sizes studied there. In spite of these expectations, we have seen that the DMRG results are not consistent

with quasi long-range order.

In this section we will show that a good qualitative description of the DMRG results can in fact be obtained from a purely classical treatment of a low-energy effective Hamiltonian describing the effects of doping the half-filled phase, a phase for which we have seen that the basic-Umklapp interaction plays a crucial role. The classical model is obtained by neglecting, by hand, the quantum fluctuations in $\phi_{+\rho}$ that if kept would have caused $\phi_{+\rho}$ to disorder on length scales $\gg 1/\delta$.

1. Classical model for the SF/DDW phase

To derive the classical model for the SF/DDW phase, we take as our starting point the low-energy effective Hamiltonian for this phase at half-filling, which will be referred to as \mathcal{H}_0 . Its form is assumed to be well approximated by the form for weak interactions, Eqs. (3.11)-(3.14), with values of the effective couplings appropriate for the system being in the SF/DDW phase for intermediate-strength interactions. In order to investigate the effects of doping, we add to \mathcal{H}_0 a chemical potential term $\Delta\mathcal{H} = -\mu\mathcal{N}$, where

$$\mathcal{N} \equiv \sum_{P\lambda s} \mathcal{N}_{P\lambda s} = \frac{2}{\pi} \int dx \partial_x \phi_{+\rho} \quad (5.25)$$

measures the number of electrons in the system with respect to the half-filled case (note that here we work with a fixed chemical potential μ instead of at a fixed doping δ as we have done up until now both in the DMRG and bosonization analyses). The fields $\phi_{+\sigma}$, $\theta_{-\rho}$, and $\theta_{-\sigma}$ are taken to be locked to values consistent with being in the SF/DDW phase, and the resulting gaps will be assumed to be large enough that excitations in these fields may be safely neglected when discussing the low-energy physics.

To obtain an effective, classical Hamiltonian from \mathcal{H}_0 we proceed as follows: (i) Neglect all terms that do not contain $+\rho$ fields, as these can be regarded as constants for our purposes. (ii) In the basic-Umklapp term (3.14), replace $\cos 2\phi_{+\sigma}$, $\cos 2\theta_{-\rho}$, $\cos 2\phi_{-\sigma}$, and $\cos 2\theta_{-\sigma}$ by their expectation values (which will generally depend on μ). This gives an effective coupling constant for $\cos 2\phi_{+\rho}$. (iii) Neglect the term containing $(\partial_x \theta_{+\rho})^2$ which gives rise to quantum fluctuations in $\phi_{+\rho}$. This makes $\phi_{+\rho}$ a purely classical field which allows us to neglect the distinction between $\phi_{+\rho}$ and $\langle \phi_{+\rho} \rangle$ in the following. Then the effective classical Hamiltonian, denoted by $\mathcal{H}_{+\rho}$, can be written

$$\mathcal{H}_{+\rho} \equiv \int_0^L dx \left[A \left(\frac{d\phi_{+\rho}}{dx} \right)^2 - B \cos 2\phi_{+\rho} \right], \quad (5.26)$$

where A and B are effective positive μ -dependent coupling constants. Since we are here considering the theory on a finite system size L , it should be noted that boundary effects have not been taken into account in this effective Hamiltonian.

We want to consider a system with a given average doping $\delta = \mathcal{N}_h/2L$, where $\mathcal{N}_h = -\mathcal{N}$ is the number of doped holes. Thus $\Delta\mathcal{H}$ is simply a constant $-2|\mu|\delta L$ which can be neglected, and $\phi_{+\rho}$ has to satisfy the boundary condition

$$\phi_{+\rho}(L) - \phi_{+\rho}(0) = -\pi\delta L. \quad (5.27)$$

Since the net spin in the z direction is measured by the operator

$$\sum_{P\lambda s} s \mathcal{N}_{P\lambda s} = \frac{2}{\pi} \int_0^L dx \partial_x \phi_{+\sigma}, \quad (5.28)$$

the fact that $\langle \partial_x \phi_{+\sigma} \rangle = 0$ in the low-energy subspace implies that the number of up- and down-spin electrons are equal. Consequently, up- and down-spin electrons are removed in pairs by the chemical potential, so that \mathcal{N}_h is an even integer, and therefore the product δL in Eq. (5.27) is an integer. Note that this condition is satisfied for all figures discussed in Sec. IV except Fig. 14 where the presence of an unpaired hole is seen to result in disturbances in the density and current patterns.

The problem we have arrived at consists in finding the function $\phi_{+\rho}(x)$ which minimizes $\mathcal{H}_{+\rho}$, subject to the boundary condition (5.27). That is, the solution $\phi_{+\rho}(x)$ is the classical ground state configuration of the sine-Gordon model in the presence of a finite density of solitons;⁸⁶ equivalently, we can think of it as a Frenkel-Kontorova-like problem.⁸⁷ There is a competition between $\mathcal{H}_{+\rho}$ which wants to lock $\phi_{+\rho}$ in one of the minima of the cosine potential, and the boundary condition which forces $\phi_{+\rho}$ to have a nonzero slope.

Once $\phi_{+\rho}(x)$ has been found, the currents and densities are easily obtained from Eqs. (3.16) and (5.1)-(5.2). It is important to note that since the doping δ is determined by the term $-\mu\mathcal{N}$ in the effective Hamiltonian, the $\delta = 0$ form of Eqs. (5.1)-(5.2) must be used. Consequently, the staggered rung current can be written

$$j_s(x) = j_0 \cos \phi_{+\rho}, \quad (5.29)$$

where $j_0 \approx j_\pi \langle \cos \phi_{+\sigma} \cos \theta_{-\rho} \cos \theta_{-\sigma} \rangle \neq 0$. The value of the amplitude j_0 will be determined by fitting to the DMRG results. Furthermore, the electron density on the top and bottom site at rung x are equal and given by

$$n(x) = 1 + \frac{1}{\pi} \frac{d\phi_{+\rho}}{dx}. \quad (5.30)$$

2. Solution of the model

To solve this problem analytically, we interpret $\mathcal{H}_{+\rho}$ as the classical *action* for a particle with mass $2A$, located at position ϕ at time x , with potential energy $B \cos 2\phi$ (here and in the rest of this paragraph we omit the subscript $+\rho$ on $\phi_{+\rho}$). It will be convenient to take the potential energy to be $V(\phi) \equiv B(\cos 2\phi - 1) = -2B \sin^2 \phi \leq 0$

corresponding to a redefinition of its zero. The sum of kinetic and potential energies is conserved,

$$A \left(\frac{d\phi}{dx} \right)^2 + V(\phi) = E, \quad (5.31)$$

where E is the total energy of the particle. According to Eq. (5.27), in the time interval L the particle moves a distance $\pi\delta L$, which (since $L > 1/\delta$) is bigger than π , the distance between the potential minima. Thus the particle is not trapped inside one of the wells of the potential $V(\phi)$, but is unbounded. Hence $E > 0$, so that the velocity $d\phi/dx$ always has the same sign, which must be negative since $\phi(L) < \phi(0)$. Eq. (5.31) can then be integrated to give

$$x - x_0 = -\sqrt{a} F(\phi | -2b), \quad (5.32)$$

where $a \equiv A/E$, $b \equiv B/E$, $F(\phi|m)$ is the incomplete elliptic integral of the first kind (see Appendix C), and x_0 is an integration constant defined by $\phi(x_0) \equiv 0$. This gives

$$\phi(x) = \text{am} \left(-\frac{x - x_0}{\sqrt{a}} \middle| -2b \right), \quad (5.33)$$

where $\text{am}(u|m)$ is the Jacobian amplitude function. Using Eqs. (5.27), (5.33), and (C4), and the assumption that L is an integer multiple of $1/\delta$, the parameters a and b can be related as

$$\frac{1}{\sqrt{a}} = 2\delta K(-2b), \quad (5.34)$$

where $K(m)$ is the complete elliptic integral of the first kind.

The staggered rung current $j_s(x)$ and electron density $n(x)$ can then be expressed in terms of the Jacobian elliptic functions cn and dn , respectively:

$$j_s(x) = j_0 \text{cn} \left(\frac{x - x_0}{\sqrt{a}} \middle| -2b \right), \quad (5.35)$$

$$n(x) = 1 - \frac{1}{\pi\sqrt{a}} \text{dn} \left(\frac{x - x_0}{\sqrt{a}} \middle| -2b \right). \quad (5.36)$$

Using Eq. (5.34) to eliminate a , we see that $n(x)$ can be expressed in terms of the unknown parameters b and x_0 , while for $j_s(x)$ an additional parameter j_0 is also needed. The parameter x_0 plays the role of a phase variable which distinguishes between different solutions related by translation along the x axis, which all have the same energy since we have neglected boundary effects.

Using Eqs. (5.34)-(5.36) and the properties of the elliptic functions, the following results are easily established: $n(x)$ and $j_s(x)$ oscillate with wavelengths $1/\delta$ and $2/\delta$, respectively, and $n(x)$ is minimal where $j_s(x)$ changes sign, i.e. at the anti-phase domain walls in the current pattern. We emphasize that these properties of the analytical solution are independent of the actual values of the fitting parameters b , j_0 and x_0 , and are in excellent agreement with the numerical DMRG results.

3. Fits to DMRG results

In Fig. 17 we show fits of the analytical expressions for $j_s(x)$ and $n(x)$ to DMRG results for a 200-rung ladder for $\delta = 0.02$ (upper panel) and $\delta = 0.04$ (middle panel). The corresponding solutions of $\phi_{+\rho}(x)$ are also shown (lower panel). For both dopings, the model parameters, and therefore the DMRG results, are identical to those in Fig. 16. The fit is rather good for $\delta = 0.04$, the main deviations occurring near the boundaries due to the neglect of boundary effects in the analytical solution. However, since by construction both the numerical and analytical curves for $n(x)$ integrate to half the total number of electrons, deviations between the density curves near the boundaries inevitably imply some deviations also away from the boundaries. These deviations come mainly in the form of a horizontal shift between the density curves which decreases towards the center of the ladder. There is an identical shift between the current curves so that the zeros of the current are always at the minima of the density. It is as if the boundaries exert a “push” on the density and current oscillations, and this effect cannot be captured by the analytical solution.

Similar features are observed in the fit for the lower doping $\delta = 0.02$, but now there are also more pronounced differences between the shapes of the analytical and numerical curves. In the analytical fit the current oscillations have a more rectangular shape and the density minima are deeper. It is natural to attribute these differences primarily to the omission of quantum fluctuations in the effective model. The step-like nature of the solitons in the analytical solution for $\phi_{+\rho}(x)$ becomes more pronounced with decreasing doping δ (see lower panel in figure), as the ratio of the soliton separation $1/\delta$ to the soliton width becomes larger. We expect that quantum fluctuations will be more efficient in smoothing the solitons the more step-like these solitons are. This picture is consistent with the reduced quality of the fit as the doping is reduced from 0.04 to 0.02.⁸⁸ Comparison with the DMRG results in Fig. 17 thus seems to suggest that while the solitons in $\phi_{+\rho}(x)$ would not be much affected by the inclusion of quantum fluctuations in the effective model for $\delta = 0.04$, they would be somewhat smoothed for $\delta = 0.02$, leading to less rectangular current oscillations and not so deep minima in the electron density.

4. The CDW and doped D-Mott phase

The results for the charge density oscillations in the CDW and doped D-Mott phase that follow from such a classical approach are also in good qualitative agreement with the DMRG results. In the CDW phase, the density on leg ℓ of rung x takes the form (obtained from Eq. (5.2) with $\delta = 0$)

$$n_{t,b}(x) = 1 + \frac{1}{\pi} \frac{d\phi_{+\rho}}{dx} \pm \tilde{n}_0 (-1)^x \cos \phi_{+\rho} \quad (5.37)$$

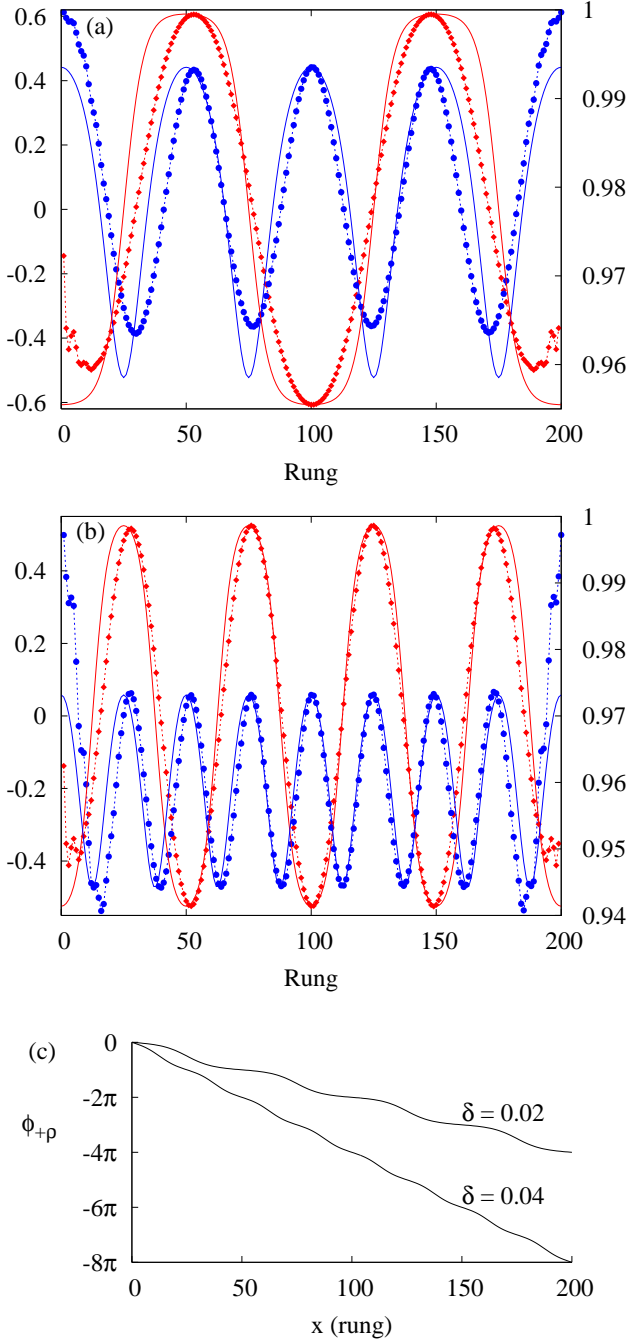


FIG. 17: (Color online) (a) Staggered rung current $j_s(x)$ (red curves, left y-axis) and electron density per site $n(x)$ (blue curves, right y-axis) as a function of rung index x in the SF/DDW phase of a 200-rung ladder with $\delta = 0.02$. Shown are DMRG results (diamonds and circles for currents and densities, respectively, connected by dashed lines to guide the eye) and analytical fits (full lines). The model parameters for the DMRG calculation are $t = V_{\perp} = 1$, $U = 0.25$, $J_{\perp} = 1.5$ and $J_{\parallel} = V_{\parallel} = 0$. The values of the fitting parameters used are $b \approx 20.0$, $|j_0| \approx 0.61$, and $x_0 = 0$. (b) Plots for the same model parameters as above, except that the doping $\delta = 0.04$. The values of the fitting parameters are $b \approx 1.66$, $|j_0| \approx 0.52$, and $x_0 = 0$. (c) The function $\phi_{+\rho}(x)$ corresponding to the fits of $j_s(x)$ and $n(x)$.

where $\tilde{n}_0 \approx n_{2k_F} \langle \cos \phi_{+\sigma} \sin \theta_{-\rho} \cos \theta_{-\sigma} \rangle \neq 0$. In the doped D-Mott phase the density also has this form except that $\tilde{n}_0 = 0$. In both phases the solution for $\phi_{+\rho} = 0$ is given by Eq. (5.33), as in the SF/DDW phase. Thus $(4k_F, 0)$ density oscillations with period $1/\delta$, coming from the $d\phi_{+\rho}/dx$ term, are predicted to be present in all phases (for the CDW phase, the DMRG results show that the $(2k_F, \pi)$ density oscillations dominate over the $(4k_F, 0)$ oscillations in size, however). Furthermore, because DMRG suggests that $\phi_{+\rho}$ essentially behaves like a classical field over the length scales considered here, the conjugate field $\theta_{+\rho}$ is strongly fluctuating, so that DSC correlations decay exponentially over these length scales even in the doped D-Mott phase.

VI. SUMMARY AND DISCUSSION

In this paper we have studied a generalized Hubbard model on a two-leg ladder, focusing on a parameter region that shows SF/DDW order. The approximate location of this region in parameter space was found from a calculation of the phase diagram of the half-filled model for weak interactions, which was done by using Abelian bosonization and semiclassical considerations to analyze the low-energy effective theory resulting from a one-loop RG flow.

The RG/bosonization calculations in this and previous works^{37,38,39} suggest that in order to get SF/DDW order in the generalized Hubbard ladder it is necessary (although not sufficient) to have the on-site repulsion U be less than the nearest neighbor repulsion V_{\perp} . One class of materials that may be promising for achieving a relatively small U is organic molecular crystals, due to the large size of the highest occupied molecular orbital; bringing two of these molecules close together might then conceivably give $U \lesssim V$.⁸⁹ Another way of reducing the effective U is through an on-site (Holstein) electron-phonon interaction.⁹⁰

To study (rational) hole dopings δ away from half-filling, finite-system DMRG calculations were done on ladders with up to 2×200 sites for intermediate-strength interactions. It was found that the SF/DDW phase persists up to quite high dopings (of order 10-20%) and that upon doping, currents remain large, with no evidence of decay. The rung currents oscillate with wavevector $(2k_F, \pi)$, corresponding to oscillations with wavelength $2/\delta$ in the *staggered* rung current. The currents coexist with $(4k_F, 0)$ charge density oscillations, with two doped holes per wavelength $1/\delta$, which also are not found to decay.

The factor of two ratio between the periodicities of the staggered rung current and the rung charge density, and the related fact that the maxima of the hole density are located at the anti-phase domain walls of the rung current, imply that the SF/DDW phase is an example of a phase with “topological doping.”⁹¹ In this respect, the rung current in the SF/DDW phase is the analogue

of the spin density in the so-called “stripe phases” in doped antiferromagnets, which have coexistence of spin and charge density order.⁵⁵

Charge density oscillations which do not seem to decay are also found in the neighboring CDW and doped D-Mott phases, in which currents decay exponentially. Both these phases have $(4k_F, 0)$ charge density oscillations; the CDW phase in addition has $(2k_F, \pi)$ charge density oscillations. DSC correlations decay exponentially in all phases (except possibly deep inside the doped D-Mott phase where the numerical results for the decay are more difficult to interpret).

We have shown that most of these DMRG results for the doped ladder can be qualitatively understood from weak-coupling RG/bosonization arguments. However, there is one apparent exception: The DMRG results are consistent with true long-range order in the currents in the SF/DDW phase and true long-range order charge density order in all phases. As far as we know, such a true long-range order scenario is not forbidden by any exact theorems that are directly applicable to the lattice Hamiltonian studied here; in particular, the Mermin-Wagner theorem is respected. On the other hand, the RG/bosonization arguments imply that such a scenario would require the symmetric charge field $\phi_{+\rho}$ to become locked and that this can only happen if multiple-Umklapp interactions are relevant in the RG sense. However, a calculation of the scaling dimension of these interactions suggests that they are irrelevant for the dopings considered, and thus the true long-range order scenario does not appear to be supported by the RG/bosonization arguments. These arguments further suggest a crossover from non-decaying current/charge density correlations to power-law decay at a length scale of order $1/\delta$, due to the basic-Umklapp interaction being unimportant on much longer length scales.³⁷ For the same reasons, in the doped D-Mott phase a crossover from exponential to power-law decay in the DSC correlations would be expected at the same characteristic length scale.

In light of this discrepancy between the predictions of the DMRG and RG/bosonization method for the long-range order question, a detailed scrutiny of both methods might be necessary, to see if one could possibly identify an omission or shortcoming of the conventional analysis that, if corrected, would resolve the discrepancy. While any investigations along these lines are beyond the scope of the present work, we will in the next paragraphs comment on the issues that might appear most salient.

For the DMRG method, a standard concern is whether boundary and/or finite-size effects could cause the system to appear to have true long-range order even if there in reality is none. However, the boundaries are in fact found to suppress SF/DDW order, not enhance it. Furthermore, the result of a finite-size test for Luttinger liquid behavior (quasi long-range order), that involved the evolution of the mid-ladder density with ladder length, was negative. Thus there seems to be no reason to expect the DMRG results to change qualitatively for larger

systems than we have studied here. The DMRG calculations are also “internally consistent” in the sense that the DSC correlations in the doped D-Mott phase are found to be consistent (or at least not inconsistent) with exponential decay, in agreement with the bosonization result when $\phi_{+\rho}$ is locked.

As the true long-range order scenario implies that $\phi_{+\rho}$ is gapped, it would have been desirable to use DMRG to calculate the charge gap directly, as function of ladder length, and see if it extrapolates to a nonzero value in the thermodynamic limit.⁴⁵ However, this calculation is very difficult and we have unfortunately not been able to do it.

It has been known for a long time^{71,92} that DMRG works with ansatz states of the form of matrix product states.^{93,94} Within this class of ansatz states it finds, with some qualification of no importance to the present argument, the variationally optimal state as approximation to the true ground state. One might think that this methodological bias might sometimes algorithmically favor a state that is not a good approximation to the true ground state (in the present case, suggesting long-range instead of quasi long-range order). To our knowledge there is however no known case where converged DMRG calculations have seriously misrepresented the true quantum state where it is known from other methods. Moreover, matrix product states would typically bias more in favor of shorter-ranged correlations. Yet, this scenario cannot be totally excluded.

One concern about the RG/bosonization method is to what extent its predictions can be trusted when the interactions are not weak. Wu et al. have recently argued that the quasi long-range order predictions would be expected to be valid also for the interaction strengths used in the DMRG calculations presented here although the parameters in the low-energy effective theory might be strongly renormalized.³⁷ A concrete example of the validity and usefulness of RG/bosonization arguments for analyzing a ladder with strong interactions was given in Ref. 45. In particular, for $3/8$ filling in the t - J ladder with $J/t \approx 0.25$, DMRG calculations showed evidence for a charge density wave with true long-range order; the values for $K_{+\rho}$ extracted from the DMRG results for $J/t \gtrsim 0.25$ were consistent with the critical value $K_{+\rho}^c = 0.125$ predicted by RG/bosonization for the onset of true long-range order.⁴⁵ But this example does of course not imply correctness of the weak-coupling RG/bosonization predictions in the model considered by us.

Another, much more speculative concern is whether some of the RG arguments used in this paper might break down in a more fundamental way. A scenario for the breakdown of the perturbative RG at certain quantum critical points has recently been discussed in Ref. 95. The breakdown occurs because the expansion coefficients of terms that appear in the RG equations at *two-loop* order depend singularly on a dangerously irrelevant variable, which causes them to diverge. Physically, the effect is

related to the presence of another diverging time scale in addition to the critical one. For coupled one-dimensional chains, nonlinear corrections to the dispersion (i.e., band curvature terms), which like the Umklapp interactions reflect the underlying lattice structure of the problem, do seem to behave in a way that might be characterized as dangerously irrelevant with respect to some transport properties (Coulomb drag).^{96,97} Whether as a result of this something akin to the breakdown described in Ref. 95 might occur in the model studied here is an intriguing, but at this stage highly speculative, question.

Although resolving the long-range order question is an important theoretical issue, as a practical matter it may make little difference whether there is true long-range order or only algebraic order that decays very slowly. Physical realizations of systems such as we consider in this paper will either involve weakly coupled ladders, or a full two-dimensional lattice. If isolated ladders can only show quasi-long-range ordered current and charge density correlations, even extremely weak coupling between such ladders could suffice to stabilize true long-range order. We note that recent results of inelastic neutron scattering measurements on $\text{Sr}_{14}\text{Cu}_{24}\text{O}_{41}$ have been interpreted as a possible signature of orbital currents.⁹⁸ Clearly it would be very interesting if further experiments on this material were to corroborate this interpretation.

Acknowledgments

We are grateful to I. Affleck, F. F. Assaad, M. A. Cazalilla, S. Chakravarty, F. H. L. Essler, E. Fradkin, A. Furusaki, T. Giamarchi, I. A. Gruzberg, A. F. Ho, S. A. Kivelson, P. A. Lee, R. H. McKenzie, A. Paramekanti, B. J. Powell, T. Senthil and M. Troyer for helpful and stimulating discussions. J. O. F. gratefully acknowledges support for this work from funds from the David Saxon chair at UCLA. For the time during which this work was being completed, he thanks the Australian Research Council for financial support, and the Rudolf Peierls Centre for Theoretical Physics at Oxford University for its hospitality. J. B. M. was supported in part by the US National Science Foundation, Grant Nos. DMR-0213818 and PHY99-0794. He also thanks the Aspen Center for Physics for its hospitality during a stay there in the summer of 2003, and MIT and the Kavli Institute for Theoretical Physics for extended stays in 2004.

APPENDIX A: KLEIN FACTOR CONVENTIONS

Here we explain the conventions used for the Majorana Klein factors^{61,64} in the bosonized versions of the Hamiltonian and the various order parameters considered in this paper.

The nonquadratic part of the Hamiltonian density, $\mathcal{H}_I^{(1b)} + \mathcal{H}_I^{(2)}$ in Eqs. (3.13)-(3.14), contains the Hermitian operator $\Gamma \equiv \eta_{1\uparrow}\eta_{1\downarrow}\eta_{2\uparrow}\eta_{2\downarrow}$. Furthermore, the bosonized

order parameters for the SF/DDW and CDW phases, Eqs. (3.15)-(3.17), contain the two anti-Hermitian operators $h_s \equiv \eta_{2s}\eta_{1s}$, $s = \uparrow, \downarrow$, while the bosonized order parameters for DSC and SSC correlations, Eqs. (3.19)-(3.20), contain the two anti-Hermitian operators $h'_\lambda \equiv \eta_{\lambda\uparrow}\eta_{\lambda\downarrow}$, $\lambda = 1, 2$. From $\Gamma^2 = -h_s^2 = -h'_\lambda{}^2 = 1$, it follows that Γ has eigenvalues ± 1 , while $\{h_s\}$ and $\{h'_\lambda\}$ have eigenvalues $\pm i$.

Since $[\Gamma, h_s] = [\Gamma, h'_\lambda] = [h_s, h_{s'}] = [h'_\lambda, h'_{\lambda'}] = 0$, it is possible to simultaneously diagonalize the order parameter of a given phase and the Hamiltonian in the Klein factor space. (Note that although $[h_s, h'_\lambda] \neq 0$, this causes no problem for such a simultaneous diagonalization, because each order parameter contains either $\{h_s\}$ or $\{h'_\lambda\}$, not both.)

A consistent choice of eigenvalues can then be deduced from the relations $\Gamma = -h_\uparrow h_\downarrow = h'_1 h'_2$. In this paper we choose the eigenvalues $\Gamma = 1$, $h_s = i$, and $h'_\lambda = i(-1)^\lambda$.

APPENDIX B: RENORMALIZATION GROUP EQUATIONS AND INITIAL CONDITIONS FOR CONTINUUM COUPLINGS AT HALF-FILLING

The one-loop RG equations can be derived using the operator product expansion (OPE).^{59,60,64,99} At half-filling they read

$$\begin{aligned}
\dot{g}_{1\rho} &= g_{t\rho}^2 + \frac{3}{16}g_{t\sigma}^2 - g_{tu1}^2 - g_{tu2}^2 - g_{tu1}g_{tu2}, \\
\dot{g}_{x\rho} &= -g_{t\rho}^2 - \frac{3}{16}g_{t\sigma}^2 - g_{xu}^2 - g_{tu1}^2 - g_{tu2}^2 - g_{tu1}g_{tu2}, \\
\dot{g}_{1\sigma} &= -g_{1\sigma}^2 - \frac{1}{2}g_{t\sigma}^2 + 2g_{t\rho}g_{t\sigma} - 4g_{tu1}^2 - 4g_{tu1}g_{tu2}, \\
\dot{g}_{x\sigma} &= -g_{x\sigma}^2 - \frac{1}{2}g_{t\sigma}^2 - 2g_{t\rho}g_{t\sigma} - 4g_{tu2}^2 - 4g_{tu1}g_{tu2}, \\
\dot{g}_{t\rho} &= 2g_{t\rho}(g_{1\rho} - g_{x\rho}) + \frac{3}{8}g_{t\sigma}(g_{1\sigma} - g_{x\sigma}) \\
&\quad - g_{xu}(g_{tu1} - g_{tu2}), \\
\dot{g}_{t\sigma} &= 2g_{t\rho}(g_{1\sigma} - g_{x\sigma}) + g_{t\sigma}(2g_{1\rho} - 2g_{x\rho} - g_{1\sigma} - g_{x\sigma}) \\
&\quad + 4g_{xu}(g_{tu1} + g_{tu2}), \\
\dot{g}_{xu} &= -4g_{x\rho}g_{xu} - g_{tu1}\left(2g_{t\rho} - \frac{3}{2}g_{t\sigma}\right) \\
&\quad + g_{tu2}\left(2g_{t\rho} + \frac{3}{2}g_{t\sigma}\right), \\
\dot{g}_{tu1} &= -g_{tu1}\left(2g_{1\rho} + 2g_{x\rho} + \frac{3}{2}g_{1\sigma} - \frac{1}{2}g_{x\sigma}\right) - g_{1\sigma}g_{tu2} \\
&\quad + g_{xu}\left(-2g_{t\rho} + \frac{1}{2}g_{t\sigma}\right), \\
\dot{g}_{tu2} &= -g_{tu2}\left(2g_{1\rho} + 2g_{x\rho} - \frac{1}{2}g_{1\sigma} + \frac{3}{2}g_{x\sigma}\right) - g_{x\sigma}g_{tu1} \\
&\quad + g_{xu}\left(2g_{t\rho} + \frac{1}{2}g_{t\sigma}\right). \tag{B1}
\end{aligned}$$

Here $\dot{g}_i \equiv 2\pi v_F dg_i/dl$, where l is related to the running cutoff scale as $\alpha(l) = \alpha e^l$. These RG equations were first

derived in Ref. 59. The initial values for the couplings are found to be

$$\begin{aligned}
g_{1\rho} &= -\frac{1}{4}U - \frac{1}{4}V_{\perp} - \frac{5}{4}V_{\parallel} + \frac{3}{16}J_{\perp} - \frac{3}{16}J_{\parallel}, \\
g_{1\sigma} &= U + V_{\perp} - V_{\parallel} - \frac{3}{4}J_{\perp} - \frac{3}{4}J_{\parallel}, \\
g_{x\rho} &= -\frac{1}{4}U - \frac{3}{4}V_{\perp} - \frac{3}{2}V_{\parallel} - \frac{3}{16}J_{\perp} - \frac{3}{8}J_{\parallel}, \\
g_{x\sigma} &= U - V_{\perp} - 2V_{\parallel} - \frac{1}{4}J_{\perp} - \frac{1}{2}J_{\parallel}, \\
g_{t\rho} &= -\frac{1}{4}U + \frac{1}{4}V_{\perp} - V_{\parallel} - \frac{3}{16}J_{\perp} - \frac{3}{8}J_{\parallel}, \\
g_{t\sigma} &= U - V_{\perp} - 2V_{\parallel} + \frac{3}{4}J_{\perp}, \\
g_{xu} &= -\frac{1}{2}U + \frac{1}{2}V_{\perp} + V_{\parallel} - \frac{3}{8}J_{\perp} - \frac{3}{4}J_{\parallel}, \\
g_{tu1} &= -\frac{1}{2}U - \frac{1}{2}V_{\perp} + \frac{1}{2}V_{\parallel} - \frac{1}{8}J_{\perp} - \frac{5}{8}J_{\parallel}, \\
g_{tu2} &= \frac{1}{2}U - \frac{1}{2}V_{\perp} - V_{\parallel} - \frac{1}{8}J_{\perp} + \frac{1}{2}J_{\parallel}. \quad (\text{B2})
\end{aligned}$$

Eqs. (B1) and (B2) hold for $t_{\perp} = t$, i.e. $k_{F2} = 2k_{F1} = 2\pi/3$. As a partial check of the internal consistency of these equations, it is instructive to generalize them to arbitrary values of t_{\perp}/t (though < 2 so that both bands are occupied) and by also allowing for density-density and spin exchange interactions along the plaquette diagonals with strength V' and J' , respectively.¹⁰⁰ It can then be shown that the generalized equations have the correct symmetries in special limiting cases: U(4) symmetry when $t_{\perp} = 0$, $U = V_{\perp}$, $V_{\parallel} = V'$, $J_{\parallel} = J_{\perp} = J' = 0$; U(2) \times U(2) symmetry when $t_{\perp} = V_{\perp} = V' = J_{\perp} = J' = 0$ (i.e. independent legs), and SO(5) symmetry when^{58,68} $J_{\perp} = 4(U + V_{\perp})$, $V_{\parallel} = V' = J_{\parallel} = J' = 0$. (Note that when $t_{\perp} = 0$ three new continuum couplings are allowed in addition to the nine present for a generic t_{\perp} .)

APPENDIX C: ELLIPTIC INTEGRALS OF THE FIRST KIND AND ASSOCIATED JACOBIAN ELLIPTIC FUNCTIONS

In this Appendix we summarize notation¹⁰¹ for and some basic properties of the elliptic integrals of the first kind and the associated Jacobian elliptic functions that are encountered in the analytical solution of the Frenkel-Kontorova-like problem in Sec. VE2.

The definitions of the incomplete and complete elliptic integrals of the first kind are, respectively,

$$F(\phi|m) \equiv \int_0^{\phi} \frac{d\alpha}{\sqrt{1 - m \sin^2 \alpha}}, \quad (\text{C1})$$

$$K(m) \equiv F(\pi/2|m). \quad (\text{C2})$$

We will only be concerned with negative values of m here. The inverse function of $u \equiv F(\phi|m)$ exists and is defined as

$$\phi \equiv \text{am}(u|m). \quad (\text{C3})$$

This function is known as the amplitude for the Jacobian elliptic functions. It is odd in u , and satisfies

$$\text{am}(u + 2K(m)|m) = \text{am}(u|m) + \pi. \quad (\text{C4})$$

The Jacobian elliptic functions encountered in our problem are

$$\text{cn}(u|m) \equiv \cos \phi, \quad (\text{C5})$$

$$\text{dn}(u|m) \equiv \frac{d\phi}{du} = \sqrt{1 - m \sin^2 \phi}. \quad (\text{C6})$$

These two functions are even and periodic in u with period $4K(m)$ for cn and $2K(m)$ for dn .

-
- ¹ B. I. Halperin and T. M. Rice, Solid State Phys. **21**, 115 (1968).
² I. Affleck and J. B. Marston, Phys. Rev. B **37**, 3774 (1988).
³ J. B. Marston and I. Affleck, Phys. Rev. B **39**, 11538 (1989).
⁴ A. A. Nersisyan and G. E. Vachnadze, J. Low Temp. Phys. **77**, 293 (1989).
⁵ H. J. Schulz, Phys. Rev. B **39**, 2940 (1989).
⁶ T. C. Hsu, J. B. Marston, and I. Affleck, Phys. Rev. B **43**, 2866 (1991).
⁷ S. Chakravarty, R. B. Laughlin, D. K. Morr, and C. Nayak, Phys. Rev. B **63**, 094503 (2001).
⁸ See, e.g., P. A. Lee, Physica C **408-410**, 5 (2004).
⁹ T. Timusk and B. Statt, Rep. Prog. Phys. **62**, 61 (1999).
¹⁰ The name “d-density wave” originates from the particle-hole nature of the condensate and the $d_{x^2-y^2}$ symmetry of its singlet order parameter; see Ref. 15.
¹¹ S. Chakravarty, H.-Y. Kee, and C. Nayak, Int. J. Mod.

- Phys. B **15**, 2901 (2001); S. Chakravarty, H.-Y. Kee, and C. Nayak, in *Physical Phenomena at High Magnetic Fields - IV*, eds. G. Boebinger, Z. Fisk, L. P. Gorkov, A. Lacerda, and J. R. Schrieffer (World Scientific, Singapore, 2002).
¹² H. A. Mook, P. Dai, and F. Doğan, Phys. Rev. B **64**, 012502 (2001); H. A. Mook, P. Dai, S. M. Hayden, A. Hiess, J. W. Lynn, S.-H. Lee, and F. Doğan, Phys. Rev. B **66**, 144513 (2002).
¹³ H. A. Mook, P. Dai, S. M. Hayden, A. Hiess, S.-H. Lee, and F. Doğan, Phys. Rev. B **69**, 134509 (2004).
¹⁴ C. M. Varma, Phys. Rev. B **55**, 14554 (1997); C. M. Varma, Phys. Rev. Lett. **83**, 3538 (1999); M. E. Simon and C. M. Varma, Phys. Rev. Lett. **89**, 247003 (2002).
¹⁵ C. Nayak, Phys. Rev. B **62**, 4880 (2000).
¹⁶ E. Cappelluti and R. Zeyher, Phys. Rev. B **59**, 6475 (1999).
¹⁷ D. A. Ivanov, P. A. Lee, and X.-G. Wen, Phys. Rev. Lett. **84**, 3958 (2000).
¹⁸ P. W. Leung, Phys. Rev. B **62**, 6112 (2000).

- ¹⁹ T. D. Stanescu and P. Phillips, Phys. Rev. B **64**, 220509 (2001).
- ²⁰ C. Nayak and E. Pivovarov, Phys. Rev. B **66**, 064508 (2002).
- ²¹ B. Binz, D. Baeriswyl, and B. Douçot, Eur. Phys. J. B **25**, 69 (2002).
- ²² A. P. Kampf and A. A. Katanin, Phys. Rev. B **67**, 125104 (2003).
- ²³ C.-H. Chung, H.-Y. Kee, and Y. B. Kim, Phys. Rev. B **67**, 224405 (2003).
- ²⁴ B. Normand and A. M. Oleś, Phys. Rev. B **70**, 134407 (2004).
- ²⁵ F. F. Assaad, Phys. Rev. B **71**, 075103 (2005).
- ²⁶ S. Capponi, C. Wu, and S.-C. Zhang, Phys. Rev. B **70**, 220505(R) (2004).
- ²⁷ For reviews, see E. Dagotto and T. M. Rice, Science **271**, 618 (1996); E. Dagotto, Rep. Prog. Phys. **62**, 1525 (1999).
- ²⁸ M. Uehara, T. Nagata, J. Akimitsu, H. Takahashi, N. Mori, and K. Kinoshita, J. Phys. Soc. Jpn. **65**, 2764 (1996).
- ²⁹ A. A. Nersesyan, Phys. Lett. A **153**, 49 (1991).
- ³⁰ A. A. Nersesyan, A. Luther, and F. Kusmartsev, Phys. Lett. A **176**, 363 (1993).
- ³¹ H. J. Schulz, Phys. Rev. B **53**, R2959 (1996).
- ³² E. Orignac and T. Giamarchi, Phys. Rev. B **56**, 7167 (1997).
- ³³ D. J. Scalapino, S. R. White, and I. Affleck, Phys. Rev. B **64**, 100506 (2001).
- ³⁴ K. Tsutsui, D. Poilblanc, and S. Capponi, Phys. Rev. B **65**, 020406 (2001).
- ³⁵ J. O. Fjærestad and J. B. Marston, Phys. Rev. B **65**, 125106 (2002).
- ³⁶ J. B. Marston, J. O. Fjærestad, and A. Sudbø, Phys. Rev. Lett. **89**, 056404 (2002).
- ³⁷ C. Wu, W. V. Liu, and E. Fradkin, Phys. Rev. B **68**, 115104 (2003).
- ³⁸ M. Tsuchiizu and A. Furusaki, Phys. Rev. B **66**, 245106 (2002).
- ³⁹ U. Schollwöck, S. Chakravarty, J. O. Fjærestad, J. B. Marston, and M. Troyer, Phys. Rev. Lett. **90**, 186401 (2003).
- ⁴⁰ T. Momoi and T. Hikihara, Phys. Rev. Lett. **91**, 256405 (2003).
- ⁴¹ T. Momoi and T. Hikihara, cond-mat/0412610.
- ⁴² P. Chandra, P. Coleman, J. A. Mydosh, and V. Tripathi, Nature **417**, 831 (2002).
- ⁴³ H.-Y. Kee and Y. B. Kim, Phys. Rev. B **66**, 012505 (2002).
- ⁴⁴ M. Vojta, A. Hübsch, and R. M. Noack, Phys. Rev. B **63**, 045105 (2001).
- ⁴⁵ S. R. White, I. Affleck, and D. J. Scalapino, Phys. Rev. B **65**, 165122 (2002).
- ⁴⁶ E. Orignac and R. Citro, Eur. Phys. J. B **33**, 419 (2003).
- ⁴⁷ P. Schmitteckert and R. Werner, Phys. Rev. B **69**, 195115 (2004).
- ⁴⁸ M. Tsuchiizu and Y. Suzumura, J. Phys. Soc. Jpn. **73**, 804 (2004).
- ⁴⁹ B. Gorshunov, P. Haas, T. Rößm, M. Dressel, T. Vuletić, B. Korin-Hamzić, S. Tomić, J. Akimitsu, and T. Nagata, Phys. Rev. B **66**, 060508(R) (2002).
- ⁵⁰ G. Blumberg, P. Littlewood, A. Gozar, B. S. Dennis, N. Motoyama, H. Eisaki, and S. Uchida, Science **297**, 584 (2002).
- ⁵¹ T. Vuletić, B. Korin-Hamzić, S. Tomić, B. Gorshunov, P. Haas, T. Rößm, M. Dressel, J. Akimitsu, T. Sasaki, and T. Nagata, Phys. Rev. Lett. **90**, 257002 (2003).
- ⁵² C. Hess, H. ElHaes, B. Büchner, U. Ammerahl, M. Hücker, A. Revcolevschi, Phys. Rev. Lett. **93**, 027005 (2004).
- ⁵³ T. Vuletić, T. Ivek, B. Korin-Hamzić, S. Tomić, B. Gorshunov, P. Haas, M. Dressel, J. Akimitsu, T. Sasaki, and T. Nagata, cond-mat/0403611.
- ⁵⁴ P. Abbamonte, G. Blumberg, A. Rusydi, A. Gozar, P. G. Evans, T. Siegrist, L. Venema, H. Eisaki, E. D. Isaacs, G. A. Sawatzky, Nature **431**, 1078 (2004).
- ⁵⁵ See, e.g., E. W. Carlson, V. J. Emery, S. A. Kivelson, and D. Orgad, in *The Physics of Conventional and Unconventional Superconductors, vol. II*, eds. K. H. Bennemann and J. B. Ketterson (Springer, 2004).
- ⁵⁶ For a discussion of this point, see Ref. 20 and references therein.
- ⁵⁷ L. P. Pryadko, S. A. Kivelson, and O. Zachar, Phys. Rev. Lett. **92**, 067002 (2004).
- ⁵⁸ H.-H. Lin, L. Balents, and M. P. A. Fisher, Phys. Rev. B **58**, 1794 (1998).
- ⁵⁹ L. Balents and M. P. A. Fisher, Phys. Rev. B **53**, 12133 (1996).
- ⁶⁰ H.-H. Lin, L. Balents, and M. P. A. Fisher, Phys. Rev. B **56**, 6569 (1997).
- ⁶¹ H. J. Schulz, G. Cuniberti, and P. Pieri, in *Field Theories for Low-Dimensional Condensed Matter Systems: Spin Systems and Strongly Correlated Electrons*, edited by G. Morandi *et al.* (Springer, New York, 2000).
- ⁶² J. von Delft and H. Schoeller, Ann. Phys. **7**, 225 (1998).
- ⁶³ A. O. Gogolin, A. A. Nersesyan, and A. M. Tsvelik, *Bosonization and Strongly Correlated Systems* (Cambridge University Press, 1998).
- ⁶⁴ D. Sénéchal, cond-mat/9908262; in *Theoretical Methods for Strongly Correlated Electrons*, eds. D. Sénéchal, A.-M. Tremblay, and C. Bourbonnais (Springer Verlag, 2003).
- ⁶⁵ T. Giamarchi, *Quantum Physics in One Dimension* (Oxford University Press, 2004).
- ⁶⁶ The names D-Mott and S-Mott were introduced in Ref. 58. Note that in Ref. 39 the D-Mott and S-Mott phase were referred to as the rung singlet and site singlet phase, respectively.
- ⁶⁷ M. Troyer, H. Tsunetsugu, and T. M. Rice, Phys. Rev. B **53**, 251 (1996).
- ⁶⁸ D. Scalapino, S.-C. Zhang, and W. Hanke, Phys. Rev. B **58**, 443 (1998).
- ⁶⁹ S. R. White, Phys. Rev. Lett. **69**, 2863 (1992); Phys. Rev. B **48**, 10345 (1993).
- ⁷⁰ I. Peschel, X. Wang, M. Kaulke, and K. Hallberg (eds.), *Density-Matrix Renormalization* (Springer-Verlag, Berlin, 1998).
- ⁷¹ U. Schollwöck, cond-mat/0409292, to appear in Rev. Mod. Phys.
- ⁷² S.-W. Tsai and J. B. Marston, Phys. Rev. B **62**, 5546 (2000); T. Senthil, J. B. Marston, and M. P. A. Fisher, Phys. Rev. B **60**, 4245 (1999).
- ⁷³ The “Mott” in the name “doped D-Mott phase” is not meant to imply that the phase that results when doping the D-Mott phase is necessarily insulating. Whether or not the various rationally doped phases are insulating is one of the central questions discussed in this paper.
- ⁷⁴ F. D. M. Haldane, Phys. Rev. Lett. **47**, 1840 (1981).
- ⁷⁵ The semiclassical approximations used are $\langle \prod_i \cos \Phi_i \rangle \approx \prod_i \langle \cos \Phi_i \rangle$.

- ⁷⁶ I. Affleck, in *Physics, Geometry, and Topology*, ed. H. C. Lee (Plenum Press, 1990).
- ⁷⁷ The form of the (most relevant) Umklapp operator has already been considered in the literature for some special commensurate fillings: $n = 1/2$ (quarter-filling),^{45,46} $n = 3/4$ and $1/4$,⁴⁵ and of course $n = 1$ (half-filling). Our result for H_{2q} agrees in all cases.
- ⁷⁸ Due to the absence of particle-hole symmetry there is an additional term proportional to $v_{F1} - v_{F2}$ in the continuum model away from half-filling. Following previous treatments, we assume that this term is irrelevant, at least for sufficiently weak dopings.
- ⁷⁹ The smallest values of $K_{+\rho}$ we are aware of in the literature occur in connection with a possible charge density wave phase with true long-range order in the t - J ladder for $n = 0.75$ and $J/t \lesssim 0.25$ (i.e. corresponding to very strong interactions), for which some evidence was recently presented in Ref. 45. In this case, it is expected that $K_{+\rho} \rightarrow 0.125$ as J/t is reduced towards its critical value $(J/t)_c$ for $n = 0.75$, and that $K_{+\rho} \rightarrow 0.0625$ as $n \rightarrow 0.75$ for $J/t < (J/t)_c$.⁴⁵
- ⁸⁰ H. J. Schulz, Phys. Rev. B **59**, 2471 (1999).
- ⁸¹ H. J. Schulz, in *Strongly Correlated Electronic Materials: The Los Alamos Symposium 1993*, edited by K. S. Bedell *et al.* (Addison-Wesley, Reading, MA, 1994).
- ⁸² T. Giamarchi, Physica B **230-232**, 975 (1997).
- ⁸³ One possible objection to this conclusion is that the analysis in Sec. V C was based on weak-coupling arguments, and that the classification of the basic-Umklapp interaction as irrelevant might therefore not be valid for intermediate and strong interactions. However, as pointed out in Ref. 45, although the quantities k_{F1} and k_{F2} may be renormalized by interactions (and may not even be well defined in the interacting model), their sum is protected by the one-dimensional version of Luttinger's theorem,^{84,85} so that the relation $4k_F = 2\pi(1 - \delta)$ is expected to be exact. This suggests that the conclusions regarding the basic-Umklapp interaction should hold more generally. This should also include the order-of-magnitude estimate $1/\delta$ for the length scale signifying the crossover from insulating behavior at shorter length scales to metallic behavior at longer length scales.
- ⁸⁴ M. Yamanaka, M. Oshikawa, and I. Affleck, Phys. Rev. Lett. **79**, 1110 (1997).
- ⁸⁵ P. Gagliardini, S. Haas, and T. M. Rice, Phys. Rev. B **58**, 9603 (1998).
- ⁸⁶ D. N. Aristov and A. Luther, Phys. Rev. B **65**, 165412 (2002).
- ⁸⁷ P. M. Chaikin and T. C. Lubensky, *Principles of Condensed Matter Physics* (Cambridge University Press, 1995).
- ⁸⁸ We note that by choosing a much smaller value of the fitting parameter b in Fig. 17, the fit of the current could have been much improved, but the density oscillations in the analytical curve would have been smaller than in the numerical curve, which would not be consistent with our picture of the role of quantum fluctuations.
- ⁸⁹ B. J. Powell (private communication, 2004).
- ⁹⁰ E. Berger, P. Valášek, and W. von der Linden, Phys. Rev. B **52**, 4806 (1995).
- ⁹¹ S. A. Kivelson and V. J. Emery, Synth. Met. **80**, 151 (1996).
- ⁹² S. Östlund and S. Rommer, Phys. Rev. Lett. **75**, 19 (1995).
- ⁹³ M. Fannes, B. Nachtergaele and R.F. Werner, Comm. Math. Phys. **144**, 3 (1992).
- ⁹⁴ A. Klümper, A. Schadschneider and J. Zittartz, Europhys. Lett. **24**, 293 (1993).
- ⁹⁵ D. Belitz, T. R. Kirkpatrick, and J. Rollbühler, Phys. Rev. Lett. **93**, 155701 (2004).
- ⁹⁶ M. Pustilnik, E. G. Mishchenko, L. I. Glazman, and A. V. Andreev, Phys. Rev. Lett. **91**, 126805 (2003).
- ⁹⁷ I. A. Gruzberg (private communication, 2003).
- ⁹⁸ C. Boullier, L. P. Regnault, J. E. Lorenzo, H. M. Rønnow, U. Ammerahl, G. Dhalenne, and A. Revcolevschi, Physica B **350**, 40 (2004).
- ⁹⁹ J. Cardy, *Scaling and Renormalization in Statistical Physics* (Cambridge University Press, 1996).
- ¹⁰⁰ J. O. Fjærestad, unpublished.
- ¹⁰¹ We follow the notation in S. Wolfram, *The Mathematica Book* (Wolfram Media, 2003), 5th ed. Note that in some treatments (see, e.g., E. T. Whittaker and G. N. Watson, *A Course of Modern Analysis* (Cambridge University Press, 1927), 4th ed.) the argument list is written (u, k) instead of $(u|m)$, with $m = k^2$.